

# Metal Halide Perovskite Solar Cells by Modified Chemical Vapor Deposition

Longbin Qiu<sup>1,\*</sup>, Sisi He<sup>2</sup>, Yan Jiang<sup>3,\*</sup>, Yabing Qi<sup>4,\*</sup>

<sup>1</sup>Department of Mechanical and Energy Engineering, Southern University of Science and Technology, Shenzhen, 518055 China

<sup>2</sup>School of Science, Harbin Institute of Technology (Shenzhen), University Town, Shenzhen, Guangdong, 518055 China

<sup>3</sup>Energy Materials and Optoelectronics Unit, Songshan Lake Materials Laboratory, Dongguan, Guangdong, 523808 China

<sup>4</sup>Energy Materials and Surface Sciences Unit (EMSSU), Okinawa Institute of Science and Technology Graduate University (OIST), 1919-1 Tancha, Onna-son, Okinawa 904-0495, Japan

\*Corresponding authors: Longbin Qiu, Email: qiu lb@sustech.edu.cn; Yan Jiang, Email: jiangyan@sslab.org.cn; Yabing Qi, Email: Yabing.Qi@OIST.jp

## Abstract

Metal halide perovskite solar cells are an emerging photovoltaic technology already exhibiting great potential. The main challenges at present that hinder the application of perovskite solar cells include scalable fabrication, operational stability, and environmental impact of Pb in perovskite solar cells. Among various scalable coating techniques, modified chemical vapor deposition (CVD) is a promising technology to enable large-area and uniform coating of perovskite layers at a low cost. Modified CVD also offers many other advantages of being solvent-free, high compatibility with industrial manufacturing, and easy integration with other solar technologies to form tandem cells (or perovskite-perovskite tandem cells). In this review, we present the recent development of perovskite solar cells as well as modules prepared by modified

CVD. As a particular focus, we first discuss the differences between modified CVD and solution coating processing. Furthermore, we summarize the present results from the cost-performance analysis point of view to show the potential of modified CVD for scalable fabrication of perovskite solar cells/modules with low cost. At the end of this review, we outline several future research directions.

## **1. Introduction**

Perovskite solar cells and modules are moving step-by-step towards industrialization at a fast speed with small area cell efficiency reaching 25.5% (0.0954 cm<sup>2</sup>), large area cell efficiency of 22.6% (1.0189 cm<sup>2</sup>), and mini-module efficiency up to 20.1% (designated area 63.98 cm<sup>2</sup>).<sup>[1-2]</sup> However, we can still clearly see the gap from small area cells to modules, with a sharper decreasing efficiency with increasing of area.<sup>[3]</sup> Currently, many researchers are focusing on the fundamental issues regarding the reducing of non-radiative recombination, lowering the defect density, and optimization of the interface for charge transfer, to further reduce the energy loss and enhance the efficiency to approach its theoretical limit.<sup>[4]</sup> But to realize its eventual large-scale application, there still remain several grand challenges besides the efficiency. The first issue is the processing up-scalability, i.e., obtaining the high efficiency on large scale. Normally with the scale-up of the area, the module efficiency will decrease, with around 0.8%/decade area increase (i.e., the absolute power conversion efficiency (PCE) value decreases by about 0.8% when the device area increases by an order of magnitude).<sup>[5-6]</sup> However, for perovskite solar modules, the decay rate is larger.<sup>[3]</sup> Technologies developed to fabricate perovskite solar modules are more complicated compared with small cells. So far, solution coating process and vapor deposition process are both investigated to fabricate large-scale solar modules.<sup>[7]</sup>

Vapor deposition is a mature deposition technique in photovoltaic industry and is favorable for large-scale deposition of uniform films with conformal coating. Vapor

1 deposition includes vacuum deposition and chemical vapor deposition (CVD). Vacuum  
2 deposition normally requires a high vacuum, while CVD normally operates under low  
3 pressure or even ambient pressure. The elimination of high vacuum requirement in  
4 CVD help reduce fabrication cost. Furthermore, the modified CVD deposited  
5 perovskite films and devices showed a high stability due to the inert atmosphere or low-  
6 vacuum annealing process and the elimination of organic solvent during the perovskite  
7 deposition process.<sup>[8-12]</sup>

8

9 Till the time we write this review, there have been over 70 research publications related  
10 to modified CVD deposition of perovskite materials for optoelectronic and photovoltaic  
11 applications since the first demonstration in 2014.<sup>[8, 13-14]</sup> Modified CVD shows a great  
12 potential in fabrication of perovskite layer with large area, compositional tuning,  
13 nano/microplates single crystals,<sup>[14]</sup> nano-fibers, and patterning of perovskite films.<sup>[15]</sup>  
14 The versatile deposition of the perovskite layer by modified CVD is promising for  
15 various applications, including solar cells/modules,<sup>[16-17]</sup> light-emitting diodes,<sup>[18]</sup>  
16 photodetectors,<sup>[19-21]</sup> phototransistors,<sup>[22]</sup> resistive switching devices,<sup>[23]</sup> and so on. This  
17 review mainly focuses on the deposition of perovskite thin films by modified CVD and  
18 its application for solar cells/modules. The context of this review includes: i) various  
19 modified CVD techniques developed for the perovskite materials including the thin-  
20 film unique features and formation kinetics (**Section 2**); ii) recently developed rapid  
21 CVD for high-quality perovskite layers (**Section 3**); iii) the factors that influence the  
22 quality of perovskite layer and related techniques like doping, composition tuning to  
23 improve the quality of perovskite layers and device performance (**Section 4**); iv) the  
24 differences between solution-coated and modified CVD deposited perovskite layers  
25 (**Section 5**), especially the state-of-the-art research works focusing on perovskite layers  
26 and devices stability by the modified CVD process; v) the potential of modified CVD  
27 for textured perovskite/Si two-terminal tandem photovoltaic devices (**Section 6**); vi)  
28 the potential of modified CVD for flexible devices (**Section 7**); vii) the cost-

performance analysis and the potential of modified CVD for commercialization (Section 8); ix) the perspective and outlook for modified CVD for large area and high-efficiency perovskite solar modules (Section 9).

## 2 Modified CVD deposition of perovskite materials

Use of CVD to prepare high quality and uniform coatings have been developed for many years as a mature thin film deposition technology, and its potential to prepare perovskite materials has been demonstrated in the early stage during the development of perovskite solar cells. In 2014 Qi and coworkers developed the hybrid CVD (HCVD) method to prepare  $\text{CH}_3\text{NH}_3\text{PbI}_3$  ( $\text{MAPbI}_3$ ) films and demonstrated the first perovskite solar cells based on CVD deposited  $\text{MAPbI}_3$ .<sup>[8]</sup> This process enables independent control of deposition parameters (e.g., the carrier gas flow rate, reaction temperature, pressure, etc.) and is particularly attractive because of its up-scaling capability, industrial-level manufacturing compatibility, and high batch-to-batch reproducibility. In the same year, Xiong and coworkers reported deposition of lead halide nano-platelets on muscovite mica substrates via van der Waals epitaxy in a vapor transport CVD deposition system, and the as-grown platelets were converted to perovskites by a gas-solid hetero-phase reaction with methylammonium (MA) halide molecules.<sup>[14]</sup> Their prepared lead halide perovskite nano-platelets exhibited a high crystal quality and good optical properties.<sup>[14]</sup> Also in the same year, Lewis and O'Brien prepared films of  $\text{MAPbBr}_3$  on glass substrates using aerosol-assisted chemical vapor deposition (AACVD).<sup>[13]</sup> However, no solar cell device results were reported in these two studies.

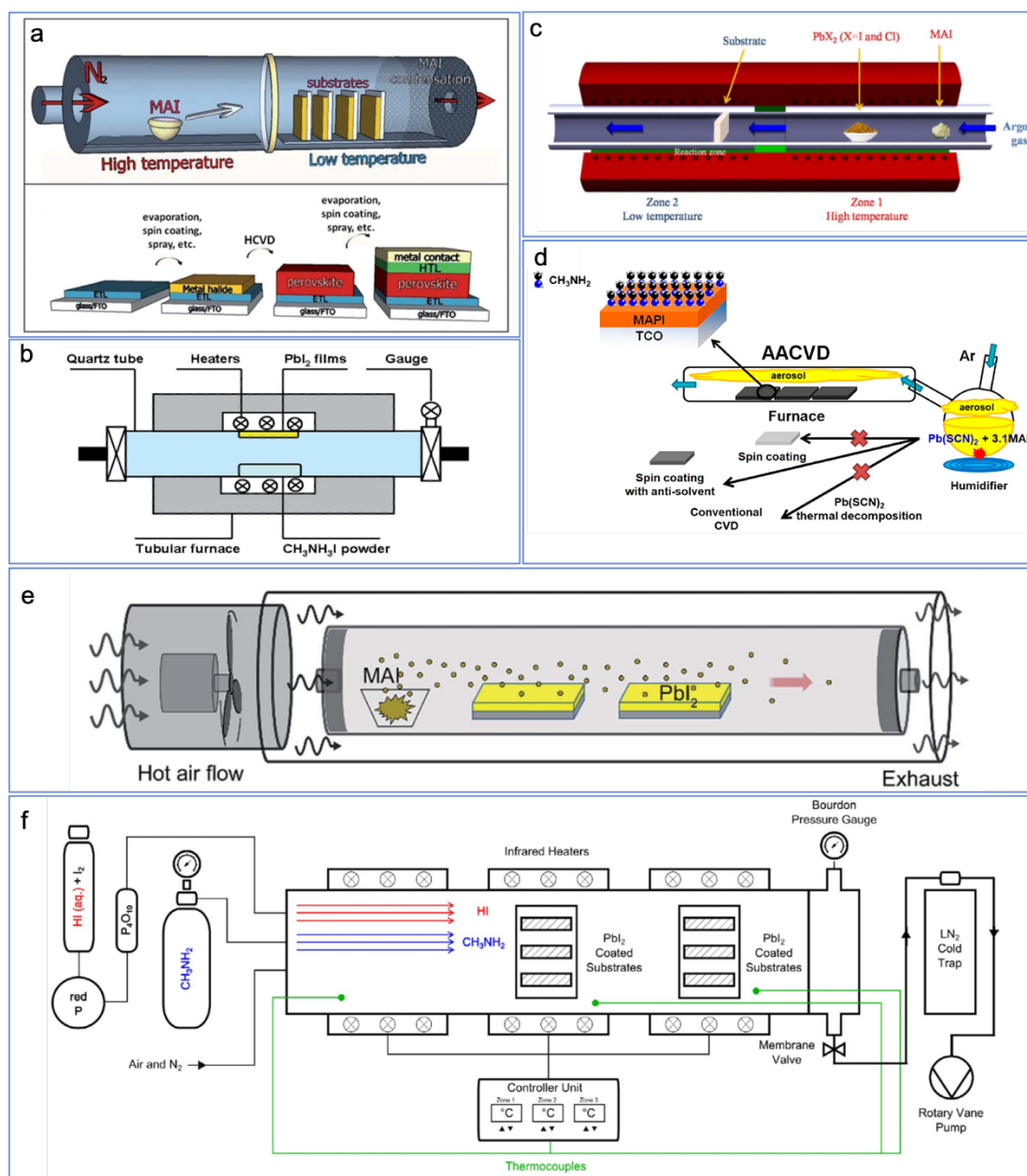
[13-14]

Based on the formation reaction mechanisms, CVD deposition of perovskite materials can be divided into several categories with different furnace designs, positions of the precursor, temperature zone control and pressure control as shown in **Figure 1**. The



1 formation of perovskite can be performed in a low vacuum or an ambient pressure  
2 condition. The precursor vapor can be sublimated from solid powder or formation of  
3 mist by ultrasonication of a precursor solution. The precursor can also be more than just  
4  $\text{PbI}_2$  and MAI but with MA gas and HI vapor for the rapid formation of perovskite  
5 materials. This section will introduce these modified CVD techniques that have been  
6 developed so far.

7



8

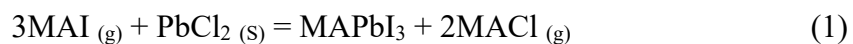
9 **Figure 1. Schematic drawing showing the various types of modified CVD to**

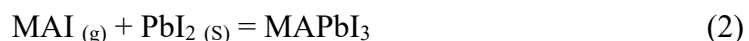
**prepare perovskite materials.** **a)** double-zone HCVD process.<sup>[8]</sup> Published by The Royal Society of Chemistry. **b)** single-zone HCVD process. Reproduced from Ref. <sup>[24]</sup> with permission from The Royal Society of Chemistry. **c)** one-step HCVD process. Reproduced from ref. <sup>[25]</sup> with permission from Springer Nature. **d)** ambient pressure AACVD process. Reproduced with permission from Ref. <sup>[26]</sup>. Copyright 2019 American Chemical Society. **e)** ambient pressure double-zone HCVD process. Reproduced from Ref. <sup>[27]</sup> with permission from The Royal Society of Chemistry. **f)** MA gas with HI vapor-based CVD process; Reproduced from Ref. <sup>[28]</sup> with permission from John Wiley & Sons.

## 2.1 Hybrid CVD (HCVD)

### 2.1.1 Double zone HCVD

In this method, the deposition of perovskite materials can be divided into two steps. The first step is the deposition of inorganic lead-containing precursors e.g., PbI<sub>2</sub>, PbCl<sub>2</sub> or PbBr<sub>2</sub>.<sup>[8]</sup> The second step is the deposition of organic halide vapor sublimated from powder precursor sources in a dedicated heating zone (**Figure 1a**),<sup>[8]</sup> which is unlike traditional CVD where the vapor precursor flows from the tube inlet. The first demonstration of HCVD of perovskite solar cells was reported in 2014 with the reaction of **equation 1**.<sup>[8]</sup> Alternatively, the inorganic precursor PbCl<sub>2</sub> can be changed to PbI<sub>2</sub> (**equation 2**). The initial trial of HCVD MAPbI<sub>3</sub> perovskite solar cells showed a PCE of 11%. Inside a furnace tube, the temperature and pressure can be designed to be uniform in an established zone, thus allowing for uniform deposition. The easy control of flowing carrier gas and pressure also guarantees the reproducibility of this coating process.





As can be seen in **Figure 1a**, there are two zones for the HCVD process, with one zone dedicated for the sublimation of organic halide precursor and the other zone for the sublimed organic halide precursor to react with the substrates that have been already pre-deposited with lead halide. In this case, the temperatures of each zone can be independently controlled. The parameters including the pressure, temperature, flowing gas and deposition time can be tuned to control the film formation. The diffusion of vapor precursor follows the relation of  $D_g \propto T^{3/2} / P$  (where  $D_g$  is the gas diffusion constant,  $T$  is the temperature, and  $P$  is the pressure). A balance between the condensing/diffusion of organic halide vapor and the reaction for the formation of perovskite should be considered. With a higher pressure and temperature in the organic precursor loaded zone, there will be a higher organic precursor vapor pressure. On the other hand, a higher organic precursor vapor pressure leads to a faster deposition of organic precursor on the  $\text{PbI}_2$  substrate in the second zone. If the condensation of organic precursor is faster than the diffusion and reaction rate with  $\text{PbI}_2$ , extra organic halide salt will be deposited, which might deteriorate the film quality. If the condensation of organic precursor is slower than the diffusion and reaction rate with  $\text{PbI}_2$ , a longer time is required for the complete formation of perovskite. The diffusion and reaction rate between organic precursor and  $\text{PbI}_2$  is determined by the temperature of the  $\text{PbI}_2$  loaded zone. By controlling the temperature of the two zones and the pressure in the tube, a balance between condensing, diffusion, and reaction for the formation of high-quality perovskite can be achieved. A more detailed mechanism is introduced in the following section.

The deposition of inorganic lead precursor film can be solution coating process or a thermal evaporation process. Because the film formation process of this inorganic lead precursor film is not a limiting factor for large area and uniform deposition of perovskite,

1 this film deposition is more flexible. With a spray-coated  $\text{PbI}_2$  as the inorganic precursor,  
2 the waste of toxic Pb could be minimized compared with vacuum deposition. Besides,  
3 a spray coating of  $\text{PbI}_2$  is suitable for large-scale deposition at a low cost. As reported,  
4 the spray-coated  $\text{PbI}_2$  combining with a double zone CVD results in uniformity and  
5 high-quality of the deposited perovskite film. Such perovskite films, when used to  
6 prepare mini-modules, showed a PCE up to 15% with an area of  $12 \text{ cm}^2$  (**Table 1**).<sup>[29]</sup>

7  
8 In a fully vapor-based deposition process, the morphology of  $\text{PbI}_2$  determines the  
9 quality of deposited perovskite films, which can be affected by the deposition rate,<sup>[30]</sup>  
10 the carrier gas and the environment.<sup>[9, 31]</sup> Deposition rates of 3.5, 4.5 and  $5.2 \text{ Å/s}$  were  
11 investigated and it was found that with a higher deposition rate, the deposited  $\text{PbI}_2$  film  
12 showed a higher degree of orientation along the (001) planes, in parallel to the  
13 substrates. Such a textured  $\text{PbI}_2$  film is beneficial for MAI vapor intercalation. A higher  
14 deposition rate also resulted in smaller  $\text{PbI}_2$  grains and a smoother surface.<sup>[30]</sup> While a  
15 lower deposition rate below  $1 \text{ Å/s}$  is expected for a compact and smooth film,<sup>[8, 16]</sup> as it  
16 is applied in most reported works, a higher deposition rate might further improve the  
17 device performance.<sup>[30]</sup> Besides the deposition rate, the carrier gas of HCVD can be  
18 ambient air with a low vacuum, as shown in **Figure 2**.<sup>[9]</sup> As reported, a post-annealing  
19 treatment is required for the complete formation of high-quality  $\text{MAPbI}_3$ .<sup>[9]</sup>

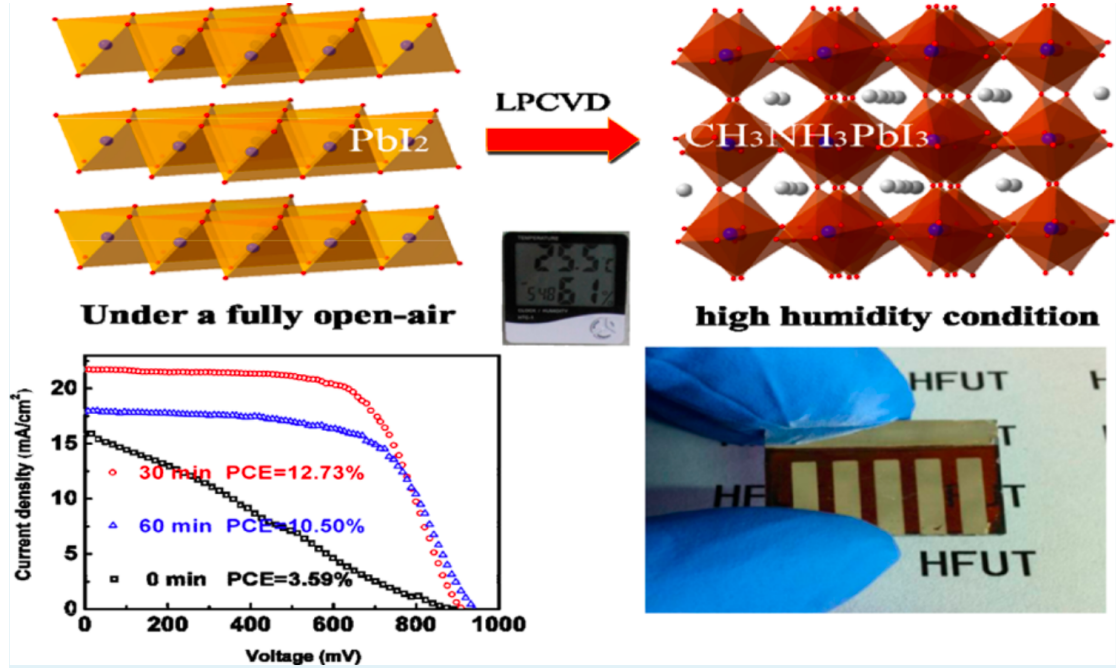
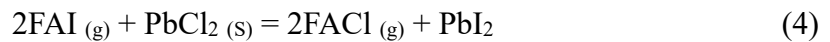


**Figure 2.** Double zone HCVD with humid air as carrier gas. A post-annealing process is required for high-performance perovskite solar cells. Reprinted with permission from ref. [9]. Copyright 2015 American Chemical Society.

The compositions of perovskite are versatile in HCVD. Because MA-based perovskite is not stable under high temperature,  $\text{CH}(\text{NH}_2)_2$  (FA) based perovskite has been intensively studied in recent years. With the replacement of MA with FA, the bandgap is reduced approaching the optimal value for single-junction solar cells. Recently pure FA-based perovskite solar cells have shown certified efficiency of 25.2%.<sup>[32-33]</sup> HCVD has also been used for fabricating large area FA-based perovskite solar cells.<sup>[34-35]</sup> The sublimation of FAI vapor and the reaction between the FAI and  $\text{PbI}_2/\text{PbCl}_2$  is crucial for forming a stoichiometric  $\text{FAPbI}_3$  film (**Equations 3 and 4**).



It is proposed that  $\text{PbCl}_2$  is a better inorganic precursor than  $\text{PbI}_2$ , because Cl is smaller and allows for easier halide exchange.<sup>[36]</sup> In addition, the presence of Cl can help

1 improve the film quality. However, it is hard to control the stoichiometry of perovskite  
2 films with vapor deposition of the organic component. The substrate loaded at different  
3 positions of the double zone furnace has different temperatures due to the temperature  
4 gradient, and the amount of deposited FAI also varies.<sup>[34]</sup> The under-saturation and  
5 over-saturation reactions happen in the near high-temperature side and near low-  
6 temperature side, respectively. Thus, precise control of deposition time and the  
7 substrate position is required. Both under-saturation and over-saturation conditions  
8 decrease the device performance. In the case of over-saturation conditions, although the  
9 prolonged annealing process can re-sublimate the over-saturated organic component  
10 and it is a reversible process, the grain size gets smaller.<sup>[34]</sup> Low-pressure vapor  
11 deposition gives precise control in film thickness and microstructure. But problems  
12 arise in controlling the stoichiometry of the inorganic-organic components as  $\text{PbI}_2$  often  
13 remains in the resulting films.<sup>[37]</sup>

14  
15 Tuning the inorganic precursor composition is an alternative strategy for perovskite  
16 composition adjusting. Considering that the Cs-FA double cation perovskite is  
17 promising for high performance, phase stable and thermal stable solar cells, co-  
18 evaporation of  $\text{CsBr/PbI}_2$  at the first stage has been reported.<sup>[16]</sup> In the second step with  
19 the deposition of FAI, a mixed cation, mixed halide perovskite  $\text{Cs}_{0.1}\text{FA}_{0.9}\text{PbI}_{2.9}\text{Br}_{0.1}$  with  
20 a large area was obtained (**Figure 3**). This is the largest reported perovskite solar  
21 module fabricated by HCVD so far (**Figures 3a and b**). The area can be readily scaled  
22 up with a larger furnace tube.

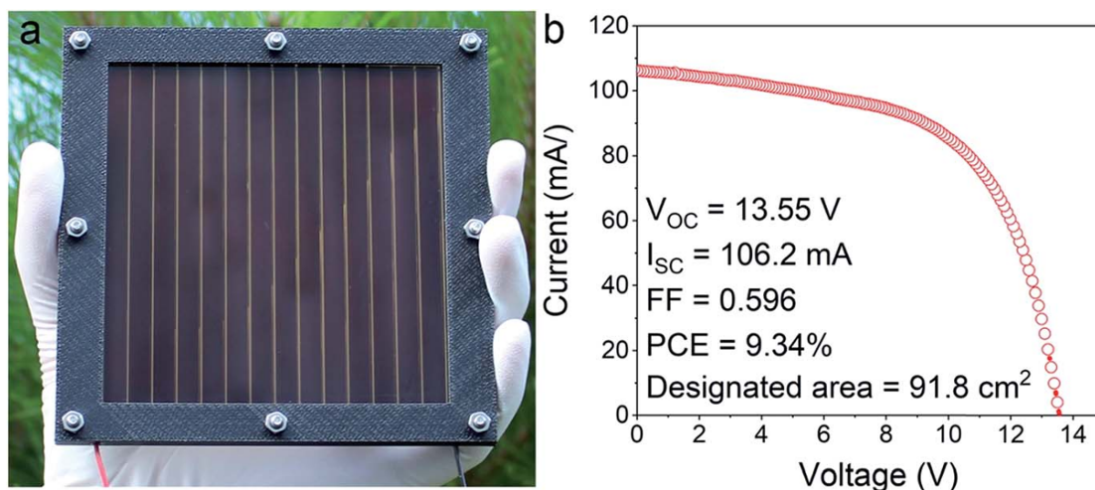


**Figure 3. a)** An optical photograph and **b)** I-V curves of a HCVD deposited perovskite solar module on a 100 cm<sup>2</sup> substrate with a designated area of 91.8 cm<sup>2</sup>.<sup>[16]</sup> Published by The Royal Society of Chemistry.

### 2.1.2 Single-Zone HCVD

Besides a double zone HCVD process design, a single zone reaction by putting the inorganic precursor thin film and organic precursor powder/film at the same position has been reported (**Figure 1b**).<sup>[24]</sup> The relative position between the inorganic and organic precursor can be face-to-face, in the vertical direction with the organic precursor in the bottom, or placed in the same horizontal plane with the organic precursor in the upstream of carrier gas.<sup>[38]</sup> This process can also be considered as a vapor-assisted solution process in a low vacuum.<sup>[39]</sup> By balancing the organic powder sublimation and reaction rate with the inorganic precursor through the control of temperature, deposition time and pressure, a series of stoichiometric perovskite films with different compositions were deposited. A single zone process is easier to operate compared with a double zone process. However, a double zone process allows the control of the sublimation of organic vapor and deposition on the substrate separately. The position and orientation of the substrate, the distance between the organic precursor and inorganic precursor are important factors influencing the film quality and device

performance, which need to be taken into account when designing experiments.<sup>[40]</sup>

A tubular furnace with a single zone for CVD was applied for the deposition of MAPbI<sub>3</sub> (**Figure 1b**). Similarly, the closed space sublimation can be considered as single zone CVD. A CsMAPbI<sub>3</sub> with efficiency approaching 20% has been achieved with the closed space sublimation by putting CsCl/PbCl<sub>2</sub> above an MAI thin film under controlled temperature.<sup>[41]</sup> Tong et al. converted a sequentially evaporated CsBr/PbI<sub>2</sub> stack with FAI for 100 minutes at 140 °C to realize a compositionally graded absorber and achieved an opaque device with a PCE of 18.2% (0.09 cm<sup>2</sup>).<sup>[42]</sup> The mixed inorganic cation species can also be introduced in the first step by a solution coating of CsI/PbI<sub>2</sub>.<sup>[43]</sup> Recently, with a homemade chamber, the mixed cation, mixed halide perovskite has been reported with the single zone CVD, which showed an efficiency up to 19.6%, which is currently the highest PCE for perovskite solar cells by CVD.<sup>[36, 44]</sup>

## 2.2 One-step CVD

A one-step CVD has been developed for the fabrication of perovskite layers (**Figure 1c**).<sup>[25]</sup> The one-step CVD is similar to one-step co-evaporation, but in a low vacuum and at a low cost. Due to the low vacuum condition, a higher temperature is required for material sublimation and vapor transport. As shown in **Figure 1c**, the schematic drawing shows the furnace for the one-step CVD. A high temperature for PbI<sub>2</sub> or PbCl<sub>2</sub> is required in the first zone. In the upstream before the high-temperature zone, the organic precursor (i.e., MAI) is loaded in a lower temperature region. Subsequently, carrying with argon gas, the PbI<sub>2</sub>/PbCl<sub>2</sub> and MAI vapor transport to the substrate in the downstream and form the perovskite.<sup>[25]</sup> For the formation of perovskite, after the deposition of inorganic and organic vapor, the substrate was annealed *in situ* in the second zone for the complete conversion. Comparing PbI<sub>2</sub> with PbCl<sub>2</sub> precursor, it is found that the presence of Cl helps minimize the morphological and energetic disorder



of the deposited film. The presence of Cl is detected in the perovskite film, which accounts for a longer carrier lifetime (**Table 1**).<sup>[25]</sup> The highest efficiency of 11.1% has been obtained by this one-step CVD. This one-step CVD is also suitable for other compositions by selecting the precursor and controlling the temperature and pressure. For example, MA<sub>3</sub>Bi<sub>2</sub>I<sub>9</sub><sup>[45]</sup> and CsPbBr<sub>3</sub><sup>[46]</sup> have been reported by one-step CVD. For the MA<sub>3</sub>Bi<sub>2</sub>I<sub>9</sub> and CsPbBr<sub>3</sub>, the sublimation temperature of the precursor is similar, thus the precursor powder can be put in more close positions.

### 2.3 Ambient pressure CVD

The ambient pressure CVD can be referred to as aerosol-assisted chemical vapor deposition (AACVD) and ambient pressure HCVD.<sup>[13, 27]</sup> AACVD is an ambient-pressure CVD technique in which that via nebulization of precursor molecules, the aerosol is transported by an inert carrier gas such as argon or nitrogen to a substrate surface (**Figure 1d**).<sup>[26]</sup> Similar to spray coating, AACVD also requires the ultrasonic vaporization of the solution and formation of mist. AACVD can be a one-step or two-step process. The one-step AACVD is to deposit the perovskite precursor with the carrier gas.<sup>[26]</sup> The two-step deposition is to deposit PbI<sub>2</sub> or PbBr<sub>2</sub> by either vapor or solution coating in the first step<sup>[13]</sup> and to react with the mist mainly consisting of the organic halide precursor, e.g., MAI, MABr, FAI, etc in the second step. In this way, the composition can be readily controlled by changing the organic halide precursor solution and the deposition takes place at a relatively low temperature. Various perovskites have been successfully deposited on glass or FTO/TiO<sub>2</sub> substrates, including MAPbBr<sub>3</sub>,<sup>[13]</sup> MAPbI<sub>3</sub>,<sup>[26, 37, 47-49]</sup> MAPb(Br<sub>1-x</sub>Cl<sub>x</sub>)<sub>3</sub>,<sup>[50]</sup> CsPbBr<sub>2</sub>I,<sup>[51]</sup> bromine doped MAPbI<sub>3</sub>,<sup>[52]</sup> and double perovskite Cs<sub>2</sub>SnI<sub>6</sub><sup>[53]</sup> by AACVD. Although AACVD has been developed in the early stage for the deposition of perovskite film, to our best knowledge, none of the deposited perovskite films has been incorporated into a working solar cell device.

Another reported ambient pressure CVD for the deposition of MAPbI<sub>3</sub> is schematically shown in **Figure 1e**.<sup>[27]</sup> The vaporization of MAI is induced by hot air at a temperature of 180 °C and with a humidity of 10%. The diffusion of MAI vapor happens from the surface to the bottom, thus the morphology of the PbI<sub>2</sub> film significantly influences the perovskite film quality, as shown in **Figure 4a**. A mesoporous PbI<sub>2</sub> is beneficial for MAI vapor diffusion and a larger grain size is obtained compared with conventional compact PbI<sub>2</sub> (**Figures 4b and c**). The perovskite layer prepared using mesoporous PbI<sub>2</sub> is also of higher quality, which showed a high PCE up to 18.90% with an active area of 0.1 cm<sup>2</sup>.<sup>[27]</sup> The mesoporous PbI<sub>2</sub> can be deposited by adding dimethyl sulfoxide (DMSO) into the PbI<sub>2</sub> precursor solution, which is better for formation of amorphous PbI<sub>2</sub> and MAI vapor diffusion.<sup>[54]</sup> However, the process might not be suitable for FAPbI<sub>3</sub> perovskite due to its sensitivity to moisture.

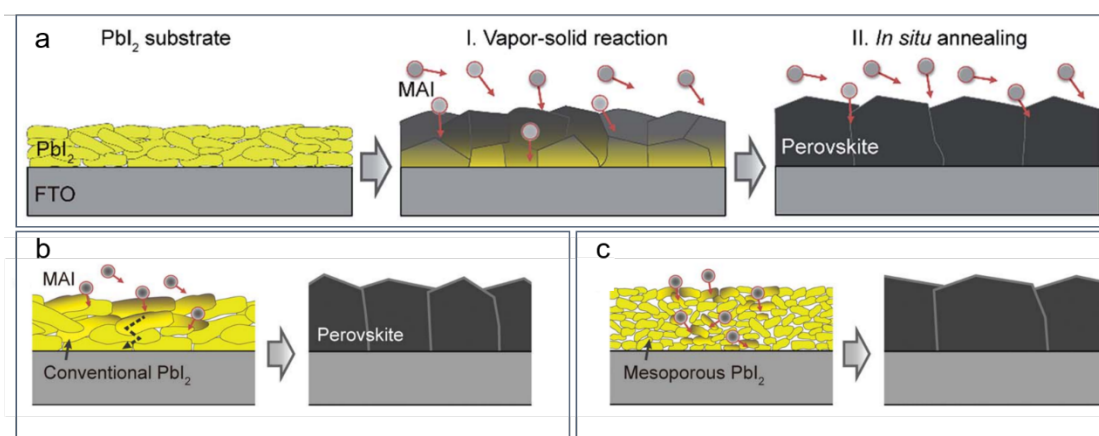


**Figure 4. a)** Perovskite formation mechanism with MAI vapor diffusing into PbI<sub>2</sub>.  
**b)** Effect of compact PbI<sub>2</sub> and **c)** mesoporous PbI<sub>2</sub> on the formation of perovskite.  
 Reproduced from ref. <sup>[27]</sup> with permission from The Royal Society of Chemistry.

## 2.4 CVD of perovskite with CH<sub>3</sub>NH<sub>2</sub> gas and HI vapor

The perovskite can be formed by a rapid reaction between PbI<sub>2</sub> and CH<sub>3</sub>NH<sub>2</sub> vapor with the assistance of moisture in ambient air or in a tube furnace in a low vacuum.<sup>[55]</sup> A systematic study and schematic drawing showing the reaction and formation of

perovskite are depicted in **Figure 5**. The reaction happens rapidly in a few seconds. The volatile and excess MA gas leaves the film, and results in a final mirror-like smooth film consists of  $\text{MAPbI}_3$  perovskite and byproducts such as  $\text{PbO}$  and  $\text{Pb(OH)}_2$ . The byproducts can be reduced by exposing one or multiple cycles of HI vapor exposure and MA vapor exposure, which can lead to higher performance in perovskite solar cells. The highest efficiency reaching 15.3% was obtained.<sup>[55]</sup>

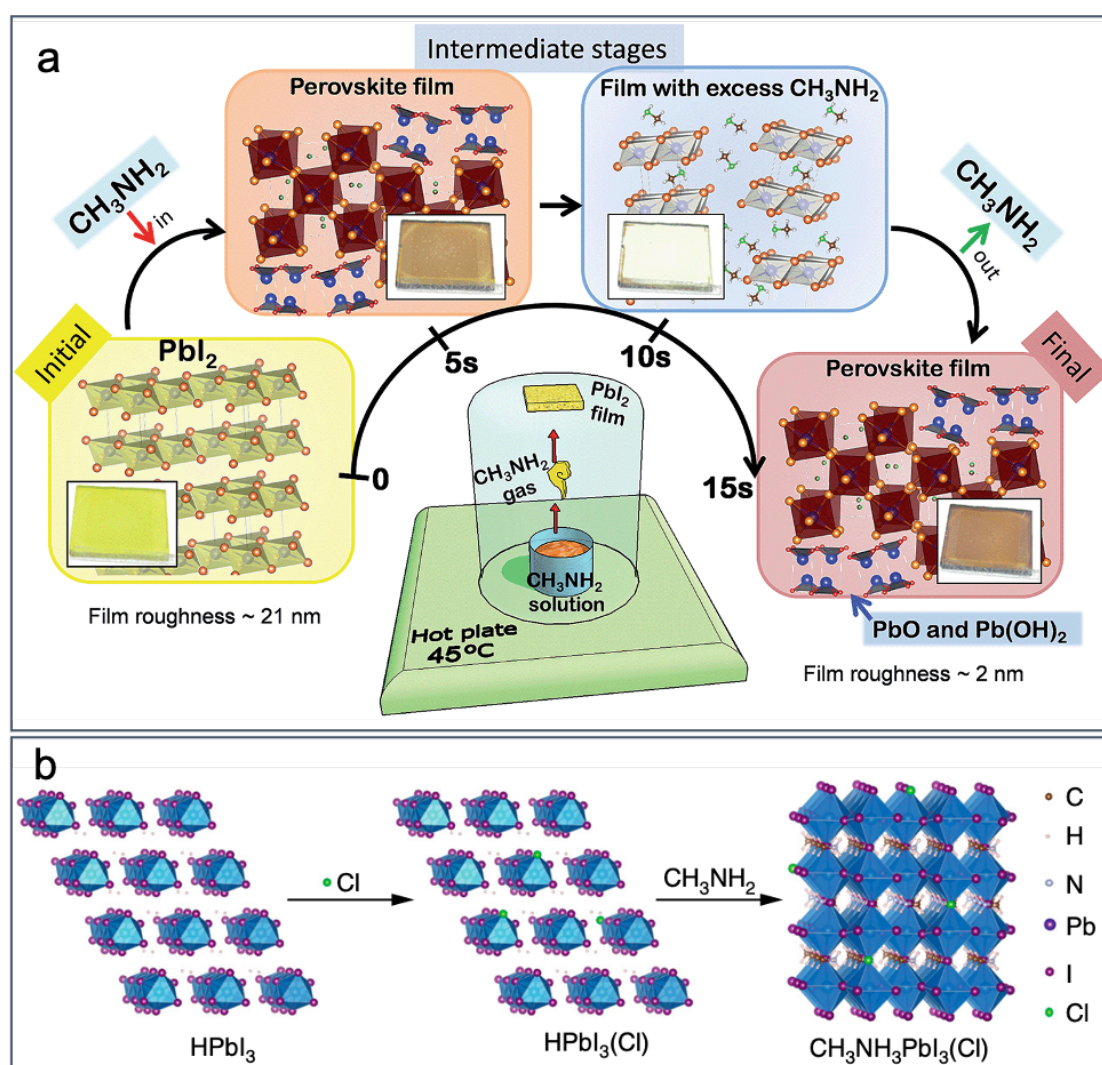


**Figure 5.** Schematic drawing showing the formation of perovskite by the reaction between **a)**  $\text{PbI}_2$  and MA gas (with the assistance of moisture in ambient air).<sup>[55]</sup> Published by The Royal Society of Chemistry. **b)**  $\text{HPbI}_3$  and MA gas. Reproduced from ref. <sup>[56]</sup> with permission from Springer Nature.

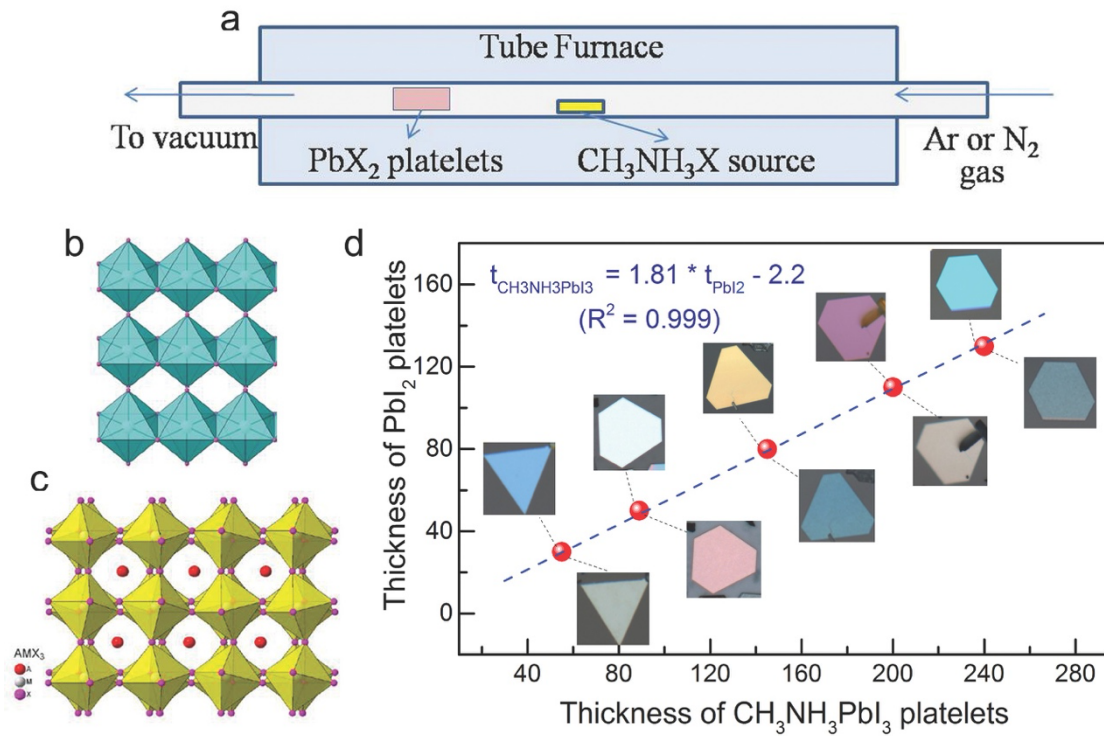
1 A modified CVD process has been designed recently based on the above-mentioned  
2 research, and the scheme of the tube furnace set-up for purging MA gas and HI vapor  
3 is shown in **Figure 1f**.<sup>[28]</sup> Considering the mechanism for the formation of perovskite  
4 by this method, a suitable humid air is required as the carrier gas. Between the purging  
5 of MA gas and HI vapor, a vacuum pumping process is applied. A PCE of 11.7% has  
6 been obtained by this CVD setup. Although the remaining PbO and Pb(OH)<sub>2</sub> in the film  
7 could not be detected by X-ray diffraction (XRD), the X-ray photoelectron  
8 spectroscopy (XPS) measurement showed that these species were present at least on  
9 the surface of the final film.<sup>[28]</sup> The purging with MA gas and HI vapor at the same time  
10 might help reduce the amount of byproducts. However, the reaction between MA gas  
11 and HI vapor for the formation of MAI is too fast to be precisely controlled before  
12 inserting the PbI<sub>2</sub> layer.<sup>[55]</sup>

13  
14 To eliminate the byproducts, an alternative strategy is to apply HPbI<sub>3</sub> as a precursor  
15 instead of PbI<sub>2</sub>.<sup>[57]</sup> The reaction between HPbI<sub>3</sub> and MA gas can form stoichiometric  
16 MAPbI<sub>3</sub> thin films, as shown in **Figure 5b**.<sup>[56]</sup> The highly volatile MA gas can easily  
17 diffuse into HPbI<sub>3</sub> for the formation of high quality and thick perovskite films. The  
18 presence of Cl can further improve the film quality at a film thickness up to 1.2 μm.  
19 The longest carrier lifetime of 500 ns is reported by this vapor-solid reaction process.  
20 PCEs of 21% for small area solar cell (0.1 cm<sup>2</sup>) and 15.3% for the solar module (12  
21 cm<sup>2</sup> active area) were obtained. More importantly, the high-quality thick film is  
22 promising for high operational stability, and the PSC maintained 90% of its initial  
23 performance after continuous AM 1.5G illumination over 2000 h.<sup>[56]</sup>

## 24 25 **2.5 CVD growth of perovskite single crystals**

26  
27 High quality perovskite films have been demonstrated by the above-summarized CVD  
28 processes. Furthermore, these CVD processes can deposit perovskite single crystals

1 with elaborate modifications.<sup>[14, 58-59]</sup> A HCVD has been applied with MAI deposition  
 2 on vacuum deposited  $\text{PbI}_2$  platelets (**Figure 6a**). The conversion happens with the  
 3 insertion of MAI into the  $\text{PbI}_2$  crystal structure accompanied by an expansion of volume  
 4 and formation of platelets such as single crystals (**Figure 6b-d**). The diffusion length  
 5 of electrons in the HCVD deposited single crystals is up to 210 nm, which is beneficial  
 6 for optoelectronic applications such as light-emitting diodes and lasers.<sup>[14]</sup> A wet  
 7 chemical and AACVD process has been applied for the synthesis of perovskite  
 8  $\text{CsPbIBr}_2$  nanosquares and deposition onto glass substrates.<sup>[51]</sup> The single crystalline  
 9 nano/micro-platelet perovskite can also be deposited by the one-step CVD process.<sup>[58]</sup>  
 10 The size of the platelets can be tuned by adjusting the  $\text{PbI}_2$  platelets/powder, MAI  
 11 powder, substrate deposition location, temperature and time in the HCVD process.<sup>[59]</sup>  
 12



13  
 14 **Figure 6. a)** Schematical drawing showing the CVD deposition of perovskite single  
 15 crystals with  $\text{PbX}_2$  platelets as the precursor. **b)** Structure of  $\text{PbX}_2$  platelets. **c)** Structure  
 16 of perovskite with the insertion of the organic halide into the crystal structure of  $\text{PbX}_2$ .  
 17 **d)** The thickness of as-deposited perovskite platelets as a function of the thickness of

PbI<sub>2</sub> platelets precursors. Reproduced from Ref. <sup>[14]</sup> with permission from Jon Wiley and Sons.

## **2.6 Formation kinetics of modified CVD deposited perovskite.**

Although various modified CVD techniques have been introduced in the previous section, the underlying principle is similar, i.e., the sublimation or vaporization of organic vapor and the transport of the vapor to the substrate pre-deposited with the inorganic precursor film. Recently the isothermal CVD process for the perovskite layers has been studied with a dual-direction pumping system. In this system, the influence of the sublimated FAI vapor during the ramping and cooling process can be avoided and the study of the kinetics for perovskite film formation is possible. The authors experimentally confirmed that the temperature of the sources and substrate influence the reaction stage. There is a balance between the FAI vapor deposition amount and the reaction rate with the bottom PbI<sub>2</sub>.<sup>[60]</sup>

Regarding the overshoot during the ramping process and the over-saturation of organic vapor, a rapid and precise heating and cooling process is required.<sup>[17]</sup> By switching the pumping direction and correspondingly changing the organic vapor flow direction, the reaction kinetics between the vapor-solid has been systematically studied (**Figure 7a and b**).<sup>[60]</sup> In this case, both ends of the furnace tube are connected to the carrier gas supply and pump, which is flexibly switched. Before reaching the stable temperature, the organic vapor is purged out directly with a carrier gas, without passing through PbI<sub>2</sub> substrate. By switching the vapor gas flow direction, the deposition of organic halide and conversion to perovskite takes place. With a precise controlling of deposition time, the gas flow is switched to a reverse direction again to prevent excess organic vapor deposition, which is beneficial for stoichiometric perovskite formation. Furthermore, the conversion kinetics of the hybrid CVD can be studied for each deposition step



(Figure 7c and d).

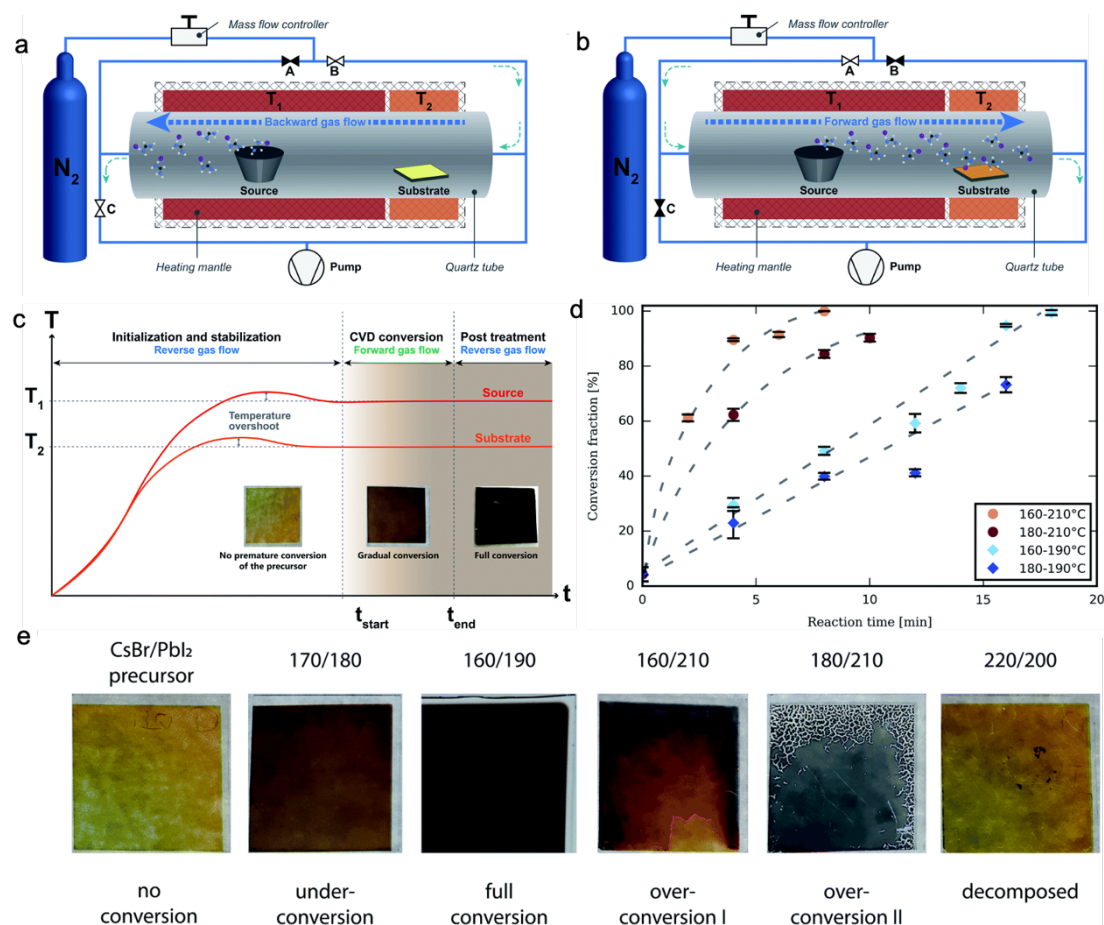


**Figure 7.** Schematic drawing showing the organic vapor gas flow direction during **a)** ramping and cooling process, and **b)** perovskite growing process. **c)** temperature profile during the HCVD process. **d)** perovskite growth kinetics with combinations of different two-zone temperatures. **e)** the conversion stages of perovskite with different temperature combinations. Reproduced from Ref. [60] with permission from The Royal Society of Chemistry.

The conversion of the perovskite can be stopped at any time by switching the vapor gas flow to a reverse direction (**Figure 7c**). The reaction progress or reaction fraction can be controlled by the reversing of gas flow direction. The reaction rate is affected by the temperature of organic sources and the temperature of substrates, as shown in **Figure 7d**. A combination of the two temperatures balances the transport of organic vapor and

the deposition and reaction of the FAI vapor and the CsBr/PbI<sub>2</sub> substrate. A 250-nm-thick CsBr/PbI<sub>2</sub> film fully converted to a high-quality perovskite within a short time of 8 min, as shown in **Figure 7c**. This is considerably short compared with the reported total process time, which includes 1 to 3 hours of annealing. The much longer process time in total is due to the slow thermal response and ramping rate, and a long thermal equilibrium time. If we only consider the reaction time, CVD is a relatively fast technique for depositing perovskite films.<sup>[60]</sup> A higher temperature of the organic source increases the reaction rate, which is due to a higher sublimation of organic vapor and faster transport to the substrate. However, a higher temperature of the substrate not always results in a higher reaction rate. This is limited by the deposition of the organic vapor and the diffusion of this organic vapor into the CsBr/PbI<sub>2</sub> layers (**Figure 7e**). This study shows a clear clue for the design of CVD setup for high quality and uniform perovskite layers. As proof of concept semi-transparent perovskite solar cell with 9.7% has been obtained without any post-treatment process.

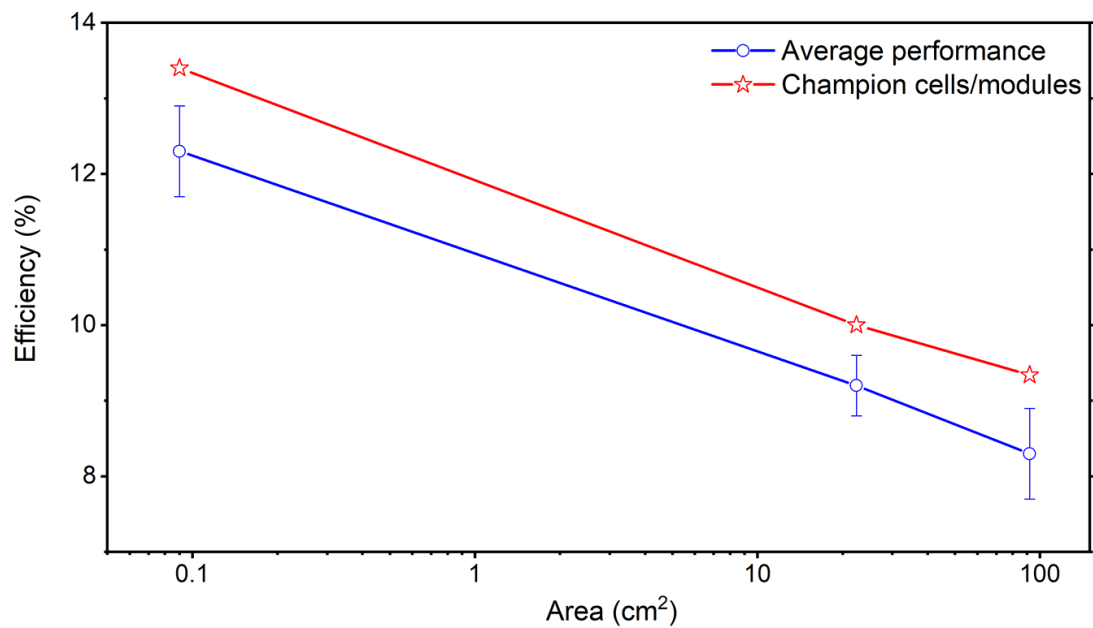
## **2.7 Scalability of modified CVD for fabricating perovskite solar cells/modules**

One of the most promising advantages of vapor deposition is scalability. As summarized in several review articles, the currently reported perovskite solar cells show markedly decreased performance with increasing area, compared with other mature photovoltaic techniques.<sup>[3, 6]</sup> The main reason is that film uniformity can not be preserved when increasing from small to large area. Modified CVD can potentially address this issue. When HCVD is used to fabricate perovskite solar modules, as the area increases from 0.1 cm<sup>2</sup> (13.4% PCE) to 91.8 cm<sup>2</sup> (designated area, 9.3% PCE) the efficiency decay rate is 1.3%/decade area (**Figure 8**). This decay slope is similar to other mature photovoltaic techniques (in the range 0.8-1.0%/decade area).<sup>[6]</sup> It is worth noting so far the cell and module efficiencies are still lower than solution-processed devices. One of the main limitations comes from the poor quality of the electron



1 transport layer (ETL) after a long time of vacuum annealing inside a tube furnace.<sup>[16-17,</sup>  
2 <sup>61]</sup> This vacuum annealing process increases the density of gap states above the valance  
3 band of the ETL and increases interface charge recombination, which deteriorates the  
4 device performance.<sup>[16-17]</sup> The vacuum annealing process will take away some oxygen  
5 from SnO<sub>2</sub> surface and deteriorates its optical/electronic properties, which forms the  
6 gap states and decreases the junction performance in solar cells.<sup>[62]</sup> These gap states are  
7 associated with Sn-5s electrons that become occupied as the surface reduces to form a  
8 Sn<sup>2+</sup> surface layer.<sup>[61, 63]</sup> With reduced vacuum deposition time, the cells (15.1% for 0.1  
9 cm<sup>2</sup>) and modules (12.3% for 22.4 cm<sup>2</sup> designated area) efficiencies both increased,  
10 although still are not comparable with the solution processed devices yet.<sup>[17, 64]</sup>

11



12

13 **Figure 8.** Solar cell efficiency decays as a function of cell/module designate area with  
14 both champion and average solar cells/modules performance.<sup>[16]</sup> Published by The  
15 Royal Society of Chemistry.

16

### 17 **3. Rapid HCVD of perovskite films**

18

19 Because the vacuum annealing process might deteriorate the quality of charge transport

layer, reduced vacuum annealing time can be beneficial. To reduce the vacuum annealing time, one needs to consider the thermal transfer processing time and annealing processing time. A possible alternative is to change the conventional heating element of filament to infrared radiation heating. The rapid thermal process has been recently developed by Qi and coworkers.<sup>[17]</sup> The ultra-fast ramping and deposition has been obtained and the CVD time has been reduced from 2-3 hours to 10 min, which is on the same order with the above-mentioned study on the HCVD kinetics.<sup>[60]</sup> **Figure 9a** shows the schematic drawing of the rapid HCVD for high-quality perovskite films, with rapid ramping, efficient annealing, and cooling, by infrared radiation and moving of heating element. In this system, the quality of electron transport layer has been better maintained, with fewer band-gap states above the valence band and hence higher electron mobility. The solar cell/module performance has been improved accordingly.<sup>[17]</sup>

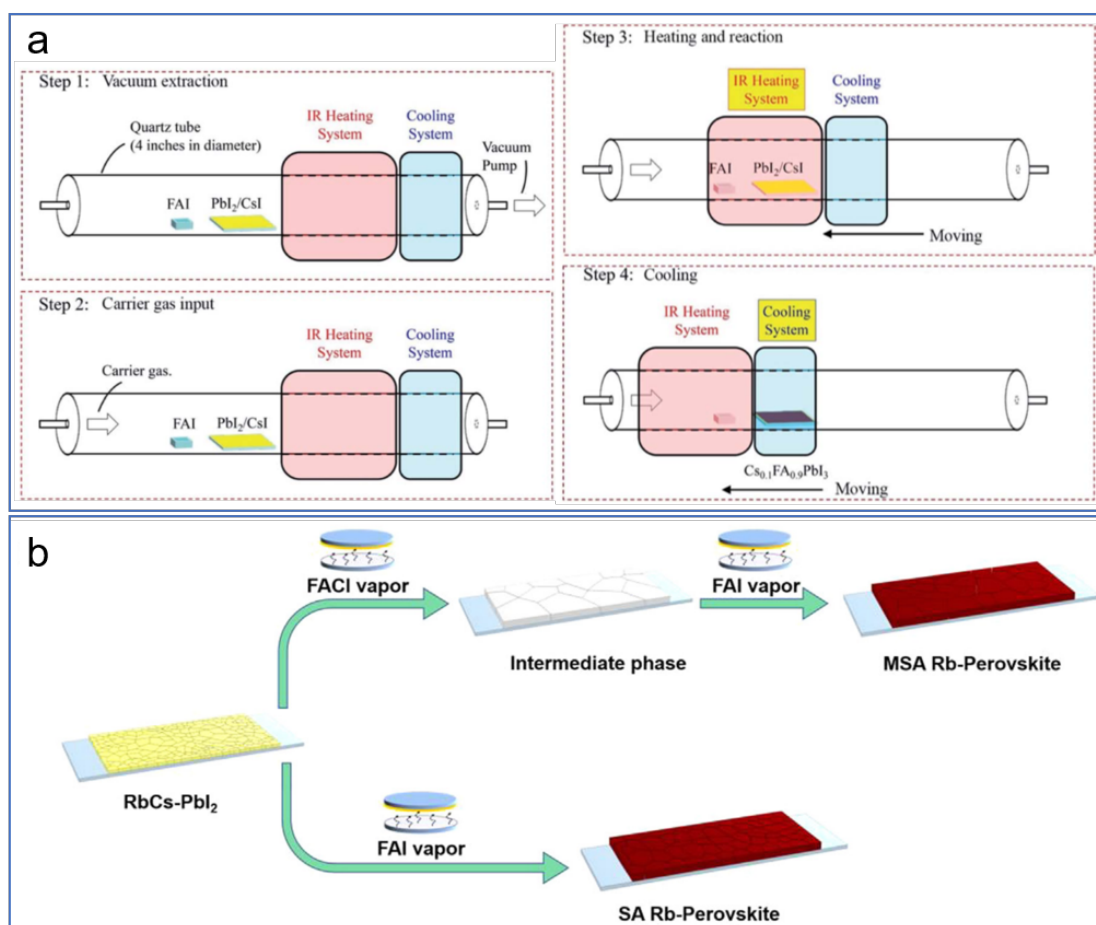


**Figure 9. a)** schematic drawing showing the steps of rapid HCVD for perovskite

1 films.<sup>[17]</sup> Published by The Royal Society of Chemistry. **b)** rapid formation of high-  
2 quality perovskite films with fast halide anion exchange process. Reprinted from Ref.  
3 <sup>[36]</sup> with permission from Elsevier.

4  
5 Another consideration for increasing the gas-solid reaction and reduction of deposition  
6 time is from the fast halide anion exchange.<sup>[36, 65]</sup> It has been reported that, with a  
7 smaller radius, chloride moves faster than iodide in a gas-solid reaction process. On the  
8 other hand, when exposed to an iodide environment, the rapid exchange between  
9 chloride and iodide happens. As shown in **Figure 9b**, with a two-step deposition, and  
10 the formation of an intermediate phase by deposition of FACl in the first step, the  
11 formation of perovskite was much faster.<sup>[36]</sup> The second step for the formation of  
12 perovskite was around 5 min. This process was used to fabricate perovskite solar cells,  
13 and an efficiency up to 19.6% was obtained (0.16 cm<sup>2</sup>). Addition of FACl with FAI in  
14 the organic vapor also improved the quality of perovskite layer and the module  
15 performance. By incorporation of FACl, perovskite solar modules with efficiencies of  
16 15% (active area of 12 cm<sup>2</sup>),<sup>[29]</sup> and 12.24% (active area of 41.25 cm<sup>2</sup>) <sup>[40]</sup> have been  
17 obtained.

#### 18 19 **4. Factors influencing the perovskite layer quality and device performance**

20  
21 Based on the above discussion, to fabricate high-quality perovskite thin films via these  
22 modified CVD methods, several factors should be taken into account: the inorganic  
23 layer morphology and composition, the thickness of the inorganic layer, the organic  
24 vapor, and the carrier gas for organic vapor.

##### 25 26 **4.1 Morphology and composition of the inorganic layer**

27  
28 For vacuum deposited PbI<sub>2</sub>, the deposition rate of PbI<sub>2</sub> influences the crystal orientation

1 and morphology. As discussed in **Section 2**, a higher deposition rate results in higher  
2 device performance.<sup>[30]</sup> On the other hand, for a solution coated PbI<sub>2</sub> film, the solvent  
3 component also influences the resulting film morphology and crystallinity. For example,  
4 by adding DMSO into the solution, a porous and amorphous PbI<sub>2</sub> film was obtained,  
5 which was beneficial for gas vapor infiltration and larger perovskite grains.<sup>[27]</sup> This PbI<sub>2</sub>  
6 precursor solution with DMSO is applied to a spray coating technique, which was used  
7 to fabricate perovskite solar modules with negligible Pb waste.<sup>[29]</sup> Addition of CsI or  
8 CsBr into the PbI<sub>2</sub> layer can help improve the phase stability of the resulting film.<sup>[16-17,</sup>  
9 <sup>43]</sup> The layer thickness of the perovskite is determined by the complete reaction of the  
10 inorganic layer, due to a diffusion barrier.<sup>[8, 34, 66]</sup>

11

12 Recently RbI, SrI<sub>2</sub>, and KI have been added into the PbI<sub>2</sub> inorganic layer to tune the  
13 composition of the resulting film.<sup>[36, 44, 65]</sup> On the other hand, a gradient composition  
14 can be formed by deposition of the CsBr/PbBr<sub>2</sub> inorganic layer with the FAI organic  
15 vapor (**Figure 10a**).<sup>[16-17, 42, 60]</sup> In this case, by using sequentially deposited CsBr and  
16 PbBr<sub>2</sub> as inorganic layer and FAI as the organic vapor source, a high quality and  
17 gradient composition perovskite film was fabricated. The resulting film consists of  
18 mainly I<sup>-</sup> as anion and the result devices showed an efficiency of 18%.<sup>[42]</sup> By adding  
19 the RbI, SrI, and KI into the PbI<sub>2</sub>, the Br anion could be stabilized during the halide  
20 exchange with FAI vapor. Mixed cation, mixed halide perovskite Cs<sub>0.14</sub>FA<sub>0.86</sub>Pb(Br<sub>x</sub>I<sub>1-</sub>  
21 <sub>x</sub>)<sub>3</sub> has been obtained with Rb, Sr or K doping. The device efficiency was up to 19.6%  
22 (**Figure 10b**).<sup>[36, 44, 65]</sup> The use of FACl to form an intermedia accelerated the halogen  
23 exchange and perovskite formation, which may help reduce the defect density in the  
24 bulk. As a result, small area cells with an efficiency of up to 19.6% have been  
25 reported.<sup>[36]</sup> This method was further applied for the fabrication of large-area modules  
26 of 16.07 cm<sup>2</sup>, which demonstrate an efficiency of 13.9%.<sup>[44]</sup> 2D perovskites have been  
27 investigated due to their higher thermal and moisture stability. As a demonstration,  
28 PEAI has been added into the PbI<sub>2</sub> layer for the following CVD of MAI. This process

formed a 2D/3D mixed perovskite with high quality and the resulting device showed an efficiency of 19.10% for a small area solar cell (Figure 10c).<sup>[67-68]</sup>

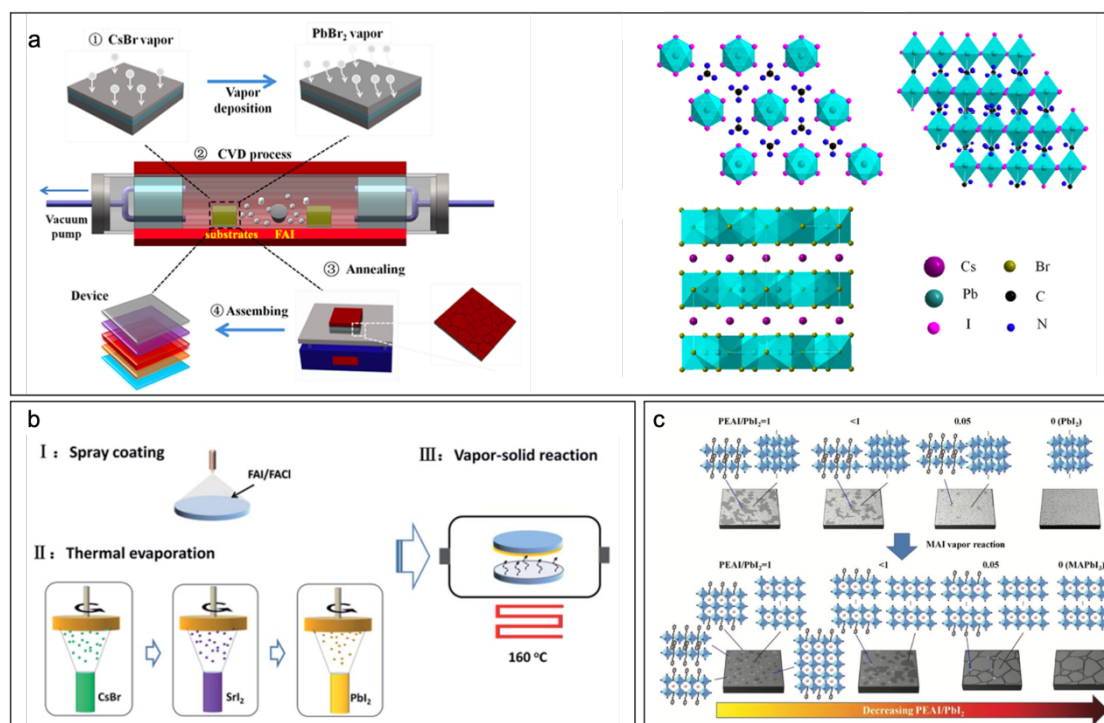


**Figure 10.** a) schematic drawing showing a sequential deposition of CsBr/PbBr<sub>2</sub> and CVD of FAI for high quality perovskite films and devices. Reprinted from Ref. <sup>[42]</sup> with permission from Elsevier. b) Mixed halide perovskite stabilized by SrI<sub>2</sub> doping and CVD deposition of FAI/FACl. Reproduced from Ref. <sup>[44]</sup> with permission from The Royal Society of Chemistry. c) 2D/3D perovskite deposited by the CVD process of MAI reacting with PbI<sub>2</sub>/PEAI. Reproduced from Ref. <sup>[67]</sup> with permission from John Wiley and Sons.

## 4.2 Carrier gas and deposition environment

Either in a low or ambient pressure, the carrier gas is an important component transporting the organic vapor to the reaction zone.<sup>[69]</sup> In most of the reported works, an inert gas such as N<sub>2</sub> or Ar has been applied as the carrier gas.<sup>[8, 34]</sup> Some of the processes used humid air as the carrier gas.<sup>[9, 27]</sup> However, in the early stage, how the

carrier gas might influence the film quality was not addressed. Mimicking dry air, a carrier gas with N<sub>2</sub>/O<sub>2</sub> (85%/15%) has been applied and compared with N<sub>2</sub>. It was demonstrated that the high-temperature HCVD process conducted in a condition of N<sub>2</sub>/O<sub>2</sub> (85%/15%) with a slow postdeposition cooling rate can successfully reduce the density of both the shallow and the deep level traps in MAPbI<sub>3</sub>, compared with a pure N<sub>2</sub> environment (**Figure 11a**).<sup>[31]</sup> A champion device with 17.6% has been achieved with the careful control of defect density and the CVD process. However, the effect of moisture and oxygen is not clear yet, although there is a study proposing that moisture and oxygen cause more defects inside the perovskite layer (**Section 5**).<sup>[70]</sup> At present, there are still different opinions regarding how the carrier gas and environment influence the film quality and defect density. Further studies will be required to clarify such effects.

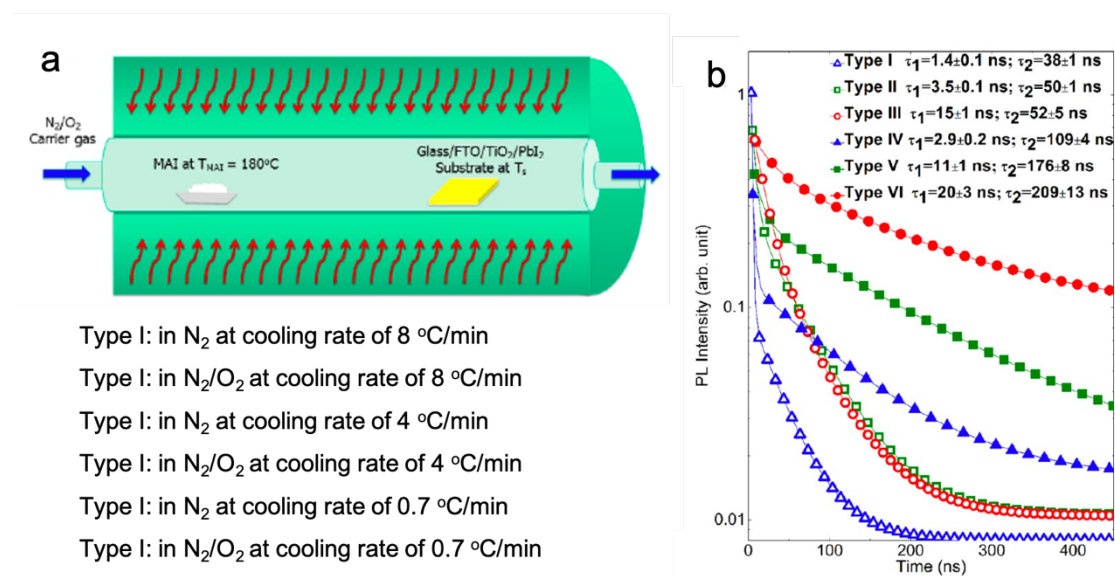


**Figure 11. a)** Schematic drawing showing a HCVD and postdeposition annealing process under different carrier gas conditions and cooling rates. **b)** Charge carrier lifetime of the perovskite films deposited in different carrier gas conditions and postdeposition cooling rates. Reprinted with permission from Ref. <sup>[31]</sup>. Copyright 2016 American Chemical Society.

1 **Table 1. Summary of the perovskite solar cells and modules fabricated by CVD. The charge carrier lifetime and operational lifetime of**  
2 **the devices have also been summarized.**

Device structure	Technique for perovskite	Area (cm <sup>2</sup> )	Efficiency (%)	V <sub>OC</sub> (V)	J <sub>sc</sub> (mA/cm <sup>2</sup> )	Fill factor	Charge carrier lifetime (ns)	Lifetime (h)	Ref
FTO/c-TiO <sub>2</sub> /m-TiO <sub>2</sub> /MAPbI <sub>3</sub> /spiro-MeOTAD/Au	Double zone-HCVD	0.09	10.8	0.92	19.1	0.62	NA	1100 <sup>s</sup>	[8]
FTO/c-TiO <sub>2</sub> /m-TiO <sub>2</sub> /FAPbI <sub>3-x</sub> Cl <sub>x</sub> /spiro-MeOTAD/Au	Double zone-HCVD	0.09	14.2	1.03	20.9	0.66	NA	155 days <sup>s</sup>	[34]
		1	7.7	0.97	18.4	0.43	NA	NA	
FTO/c-TiO <sub>2</sub> /MAPbI <sub>3</sub> /spiro-MeOTAD/Ag	Double-zone HCVD	0.12	12.73	0.91	1.7	0.645	34	NA	[9]
FTO/c-TiO <sub>2</sub> /MAPbI <sub>3-x</sub> Cl <sub>x</sub> /spiro-MeOTAD/Au	Single-zone HCVD	0.062	16.8	1.04	21.7	0.75	NA	NA	[71]
FTO/c-TiO <sub>2</sub> /MAPbI <sub>3</sub> /spiro-MeOTAD/Ag	Single-zone HCVD	0.12	12.2	0.952	21.0	0.61	NA	NA	[24]
FTO/c-TiO <sub>2</sub> /m-TiO <sub>2</sub> /MAPbI <sub>3</sub> /spiro-MeOTAD/Au	Single-zone HCVD	0.16	14.7	1.05	22.63	0.60	NA	31 days <sup>s</sup>	[38]
FTO/c-TiO <sub>2</sub> /MAPbI <sub>3</sub> /spiro-MeOTAD/Au	One-step HCVD	NA	9.2	0.95	15.9	0.61	10	NA	[25]
FTO/c-TiO <sub>2</sub> /MAPbI <sub>3-x</sub> Cl <sub>x</sub> /spiro-MeOTAD/Au			11.1	0.97	18	0.64	120		
ITO/ZnPc/MAPbI <sub>3</sub> /C <sub>60</sub> /BCP/Al	Single-zone HCVD	0.032	11.6	0.96	17.26	0.70	NA	NA	[30]

FTO/c-TiO <sub>2</sub> /m-TiO <sub>2</sub> /MAPbI <sub>3</sub> /spiro-MeOTAD/Au	Double-zone HCVD	0.09	15.6	1.06	21.7	0.68	NA	NA	[10]
FTO/c-TiO <sub>2</sub> /m-TiO <sub>2</sub> /FAPbI <sub>3</sub> /spiro-MeOTAD/Au		2.0	10.4	1.02	19.5	0.53			
		8.8	9.5	0.98	16.9	0.57			
		12.0	9.0	0.94	17.8	0.54			
FTO/c-TiO <sub>2</sub> /m-TiO <sub>2</sub> /MAPbI <sub>3</sub> /spiro-MeOTAD/Au	Double-zone HCVD	0.06	17.6	1.00	23.0	0.77	~200	NA	[31]
FTO/c-TiO <sub>2</sub> /m-TiO <sub>2</sub> /MAPbI <sub>3</sub> /spiro-MeOTAD/Au	MA gas + HI vapor	0.09	15.3	1.05	20.6	0.71	NA	133 days <sup>s</sup>	[55]
FTO/c-TiO <sub>2</sub> /m-TiO <sub>2</sub> /MAPbI <sub>3</sub> /spiro-MeOTAD/Au	Single-zone HCVD	0.24	14.99	1.04	19.19	0.74	NA	NA	[72]
FTO/c-TiO <sub>2</sub> /MAPbI <sub>3</sub> /spiro-MeOTAD/Au		0.24	15.37	0.972	21.15	0.75			
FTO/c-TiO <sub>2</sub> /m-TiO <sub>2</sub> /MAPbI <sub>3</sub> /spiro-MeOTAD/Au		8.4	6.22	2.93	3.43	0.61			
FTO/c-TiO <sub>2</sub> /m-TiO <sub>2</sub> /MAPbI <sub>3</sub> /spiro-MeOTAD/Au	Double-zone HCVD (ambient pressure)	0.11	18.90	1.06	22.08	0.80	NA	NA	[27]
ITO/PTAA/MAPbI <sub>3</sub> /PCBM/ZnO/Al	Double-zone HCVD	NA	15.4	0.955	22.7	71.0	2.4	NA	[73]
FTO/c-TiO <sub>2</sub> /m-TiO <sub>2</sub> /Cs <sub>0.15</sub> FA <sub>0.85</sub> PbI <sub>3</sub> /spiro-MeOTAD/Ag	Single-zone HCVD	0.12	14.45	0.906	22.858	0.698	NA	7 days <sup>s</sup>	[43]
FTO/c-TiO <sub>2</sub> /MAPbI <sub>3-x</sub> Cl <sub>x</sub> /spiro-MeOTAD/Au	Single-zone HCVD	0.09	11.5	0.91	18.33	0.67	NA	NA	[74]
FTO/c-TiO <sub>2</sub> /m-TiO <sub>2</sub> /Cs <sub>0.07</sub> FA <sub>0.93</sub> PbI <sub>3</sub> /spiro-	Double-zone HCVD	0.1	16.6	1.00	22.00	0.752	NA	20 °	[75]



MeOTAD/Au		12.0	14.6	5.84	3.67	0.681		NA	
FTO/c-TiO <sub>2</sub> /m-TiO <sub>2</sub> /(PEA <sub>2</sub> MA <sub>n-1</sub> Pb <sub>n</sub> I <sub>3n+1</sub> )/spiro-MeOTAD/Au	Single-zone HCVD	0.2	19.10	1.08	21.91	0.8036	NA		[67]
FTO/SnO <sub>2</sub> /Cs <sub>0.24</sub> FA <sub>0.76</sub> PbI <sub>3-y</sub> Br <sub>y</sub> /spiro-MeOTAD/Au	Single-zone HCVD	0.16	17.79	1.065	22.88	0.712	~300	NA	[40]
		41.25	12.24	9.16	2.25	0.526			
FTO/c-TiO <sub>2</sub> /CsPbBr <sub>3</sub> /Carbon	Single-zone HCVD	0.12	5.38	1.13	6.79	0.70	NA	21 days <sup>s</sup>	[76]
FTO/c-TiO <sub>2</sub> /m-TiO <sub>2</sub> /MAPbI <sub>3</sub> /spiro-MeOTAD/Au	Double-zone HCVD	0.06	16.9	1.01	24.2	0.69	NA	NA	[77]
FTO/c-TiO <sub>2</sub> /Cs <sub>0.15</sub> FA <sub>0.85</sub> PbI <sub>2.85</sub> Br <sub>0.15</sub> /spiro-MeOTAD/Au	Single-zone HCVD	0.09	18.22	1.06	22.82	0.754	NA	1400 <sup>s</sup>	[42]
FTO/c-TiO <sub>2</sub> /MAPbI <sub>3</sub> /SWCNT	Single-zone HCVD	NA	7.9	0.91	15.5	0.56	NA	500 <sup>s</sup>	[78]
FTO/c-TiO <sub>2</sub> /MAPbI <sub>3</sub> /spiro-MeOTAD/Au	Single-zone HCVD	0.09	15.5	1.03	20.46	0.73	NA	NA	[66]
FTO/c-TiO <sub>2</sub> /Cs <sub>0.1</sub> FA <sub>0.9</sub> PbI <sub>3</sub> /spiro-MeOTAD/Au	Single-zone HCVD	NA	16.39	0.99	22.87	0.7482	21	30 days	[79]
Ti/c-TiO <sub>2</sub> /m-TiO <sub>2</sub> /FAPbI <sub>3-x</sub> Cl <sub>x</sub> /spiro-MeOTAD/Au	Single-zone HCVD	0.05	10.79	0.95	15.14	0.75	NA	NA	[80]
FTO/c-TiO <sub>2</sub> /m-TiO <sub>2</sub> /FAPbI <sub>x</sub> Br <sub>3-x</sub> /spiro-MeOTAD/Au	Double-zone HCVD	0.1	16.2	1.03	21.1	0.74	NA	535 °	[29]
		2.0	16.1	1.03	21.1	0.74		NA	
		12.0	14.7	6.29	3.55	0.66		388 °	
FTO/SnO <sub>2</sub> /C <sub>60</sub> /Cs <sub>0.1</sub> FA <sub>0.9</sub> PbI <sub>2.9</sub> Br <sub>0.1</sub> /spiro-	Double-zone HCVD	0.09	13.3	0.90	20.2	0.67	40	500 °	[16]

MeOTAD/Au		91.8	9.34	13.55	1.16	0.596			
FTO/c-TiO <sub>2</sub> /m-TiO <sub>2</sub> /MABiI <sub>3</sub> /spiro-MeOTAD/Au	CVD	0.19	0.02	0.39	0.13	0.3896	NA	NA	[81]
FTO/c-TiO <sub>2</sub> /PCBM/MAPbI <sub>3</sub> /spiro-MeOTAD/Au	Single-zone HCVD	0.09	12.2	0.922	18.7	0.71	NA	NA	[82]
FTO/SnO <sub>2</sub> /Cs <sub>0.24</sub> FA <sub>0.76</sub> PbI <sub>3-y</sub> Br <sub>y</sub> (SrI)/spiro-MeOTAD/Au	Single-zone HCVD	0.16	17.66	1.021	21.96	0.789	NA	60 days <sup>s</sup>	[44]
		16.07	13.92	6.280	3.29	0.674	NA	NA	
FTO/c-TiO <sub>2</sub> /C <sub>60</sub> /(PEA <sub>2</sub> MA <sub>n-1</sub> Pb <sub>n</sub> I <sub>3n+1</sub> )/spiro-MeOTAD/Au	Single-zone HCVD	NA	18.08	1.08	23.75	0.704	NA	30 days <sup>s</sup>	[68]
FTO/c-TiO <sub>2</sub> /m-TiO <sub>2</sub> /MAPbI <sub>3</sub> /spiro-MeOTAD/Au	MA gas + HI vapor	0.325	12.9	1.04	18.6	0.67	NA	NA	[28]
ITO/PTAA/Cs <sub>0.24</sub> FA <sub>0.76</sub> PbI <sub>3-y</sub> Br <sub>y</sub> /ZnO/AZO/Ni-Al-grid	Double zone HCVD	0.27	10.6	0.95	17.5	0.6	55	NA	[60]
FTO/SnO <sub>2</sub> /Cs <sub>0.1</sub> FA <sub>0.9</sub> PbI <sub>3</sub> /spiro-MeOTAD/Au	Double zone HCVD	0.1	15.5	0.99	22.3	0.702	NA	NA	[17]
		22.4	12.3	6.8	2.7	0.672			
FTO/SnO <sub>2</sub> /Rb <sub>0.04</sub> Cs <sub>0.14</sub> FA <sub>0.86</sub> Pb(Br <sub>x</sub> I <sub>1-x</sub> ) <sub>3</sub> /spiro-MeOTAD/Au	Single zone HCVD	0.148	19.59	1.127	22.63	0.768	~270	NA	[36]
		10.0	15.13	6.243	3.51	0.70			
FTO/SnO <sub>2</sub> /Rb <sub>0.04</sub> Cs <sub>0.14</sub> FA <sub>0.86</sub> Pb(Br <sub>x</sub> I <sub>1-x</sub> ) <sub>3</sub> /spiro-MeOTAD/Au	Single zone HCVD	0.16	19.6	1.13	22.20	0.78	~150	NA	[65]

1 c-TiO<sub>2</sub>: compact TiO<sub>2</sub> layer. m-TiO<sub>2</sub>: mesoporous TiO<sub>2</sub>. <sup>s</sup>: storage stability. <sup>o</sup>: operational stability

2 V<sub>OC</sub>: Open-circuit voltage; J<sub>SC</sub>: Short-circuit current

## 5. Difference between modified CVD deposited perovskite films and solution coated perovskite films

Although modified CVD has the potential for scalable fabrication of perovskite solar modules, the device efficiency still lags behind those based on the solution processes. Understanding the differences between solution-coated and CVD fabricated perovskite films is important for the development of CVD based large-scale and high-performance modules. So far only a few reports focus on the film properties by CVD and solution coating processes.<sup>[77]</sup> Recently, the film quality and stability based on different coating techniques have been studied systematically. As shown in **Figure 12a**, there are five coating processes for MAPbI<sub>3</sub> considering the coating techniques and environment.<sup>[70]</sup> It is found that a full vacuum process and CVD process in an inert N<sub>2</sub> environment showed the most stable films under continuous light illumination. The films fabricated in air or other two-step methods showed a fast degradation rate under light illumination.<sup>[70]</sup> The steady-state photoluminescence (PL) spectra also showed the highest intensity for the CVD based film (**Figure 12b**). By varying the laser power for the steady-state PL measurement, the slope of the PL intensity as a function of laser power provides the information regarding the defect states inside the coated films (**Figure 12c**). A slope close to 2 means that both negative and positive charge carriers are trapped. With a slope close to 1.5, either holes or electrons are trapped. A slope close to 1 indicates exclusive free carrier recombination and thus a very small number of defects and traps.<sup>[83]</sup> The authors claimed that the fabrication in an inert environment could reduce the defect states, as shown in **Figure 12d**.<sup>[70]</sup> The CVD based process showed the most stable perovskite films,<sup>[84]</sup> which is consistent with previous reports.<sup>[8-9]</sup> For FAPbI<sub>3</sub>, the film also showed higher phase stability under a humid environment.<sup>[34]</sup> However, this cannot explain why the performance of the device based on HCVD is lower than the solution-based methods.<sup>[10]</sup>

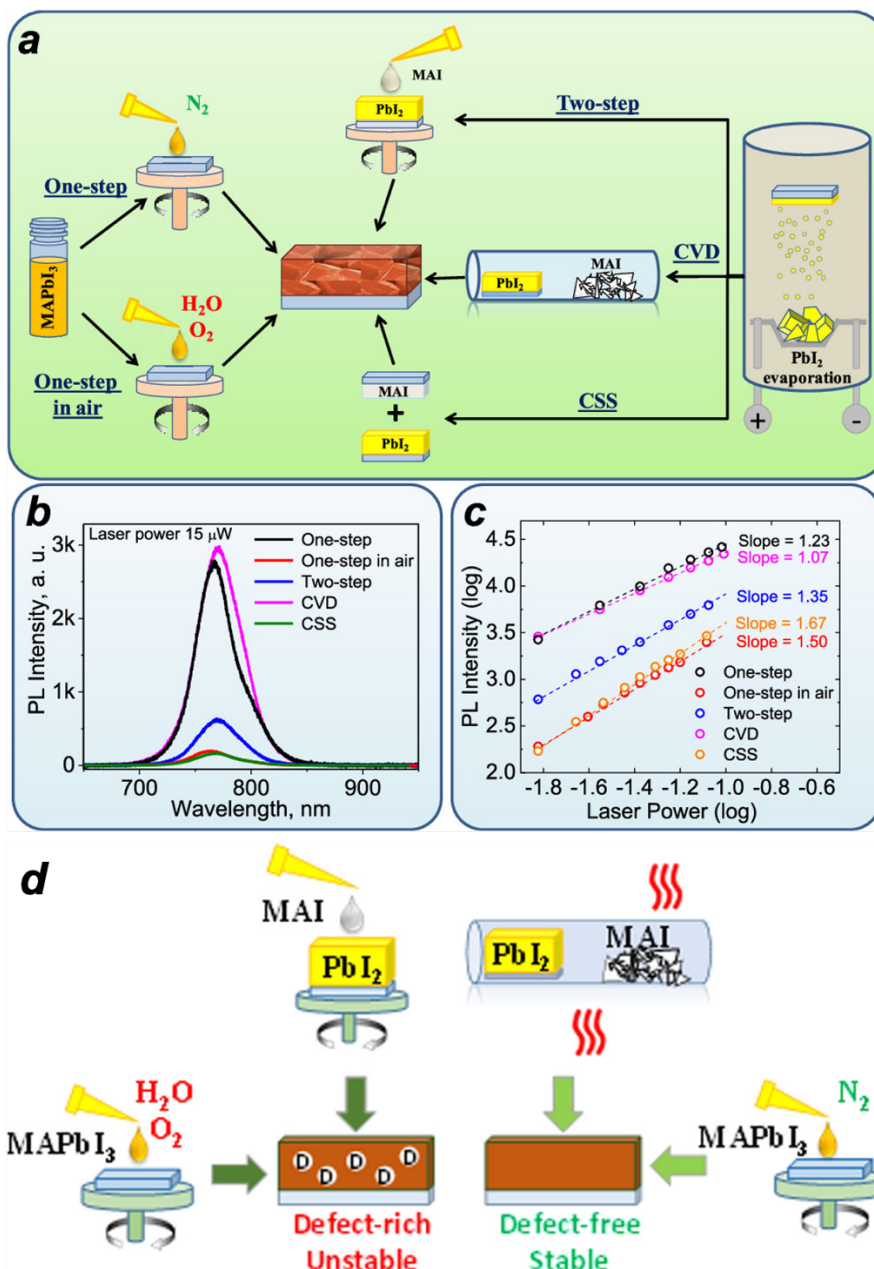


**Figure 12.** **a)** Schematic drawing showing the various deposition processes for depositing perovskite films. **b)** PL spectra of perovskite films deposited by various methods. **c)** PL intensity of perovskite films deposited by various methods as a function of laser power. **d)** Schematic drawing showing the defects inside perovskite films deposited by various methods. Reprinted with permission from Ref. [70]. Copyright 2020 American Chemical Society.

On the other hand, by summarizing the data in **Table 1**, we can hypothesize that one of

the main differences between solution-coated and modified CVD deposited perovskite films may be the crystal quality, which leads to different carrier lifetimes. The much shorter lifetime of CVD deposited films causes a lower open-circuit voltage.<sup>[4]</sup> It can be seen that CVD deposited perovskite layer has a typical carrier lifetime in the range of 10 to 100 ns, which is shorter than solution-coated perovskite films. **Table 1** summarizes the perovskite solar cells based on CVD techniques. The related photovoltaic parameters and perovskite film carrier lifetimes have also been listed. We can see that the carrier lifetime and open-circuit voltage ( $V_{OC}$ ) are relatively low compared with other reported solution-coated films. Based on the carrier lifetime, the maximum open-circuit voltage can be calculated. For example, a  $CS_{0.1}FA_{0.9}PbI_{2.9}Br_{0.1}$  perovskite with 40 ns lifetime has a maximum  $V_{oc}$  of 1.04 V (**Figure 13**).<sup>[16]</sup> As a comparison, a solution-coated perovskite layer, the carrier lifetime can be up to 500 ns.<sup>[85]</sup>

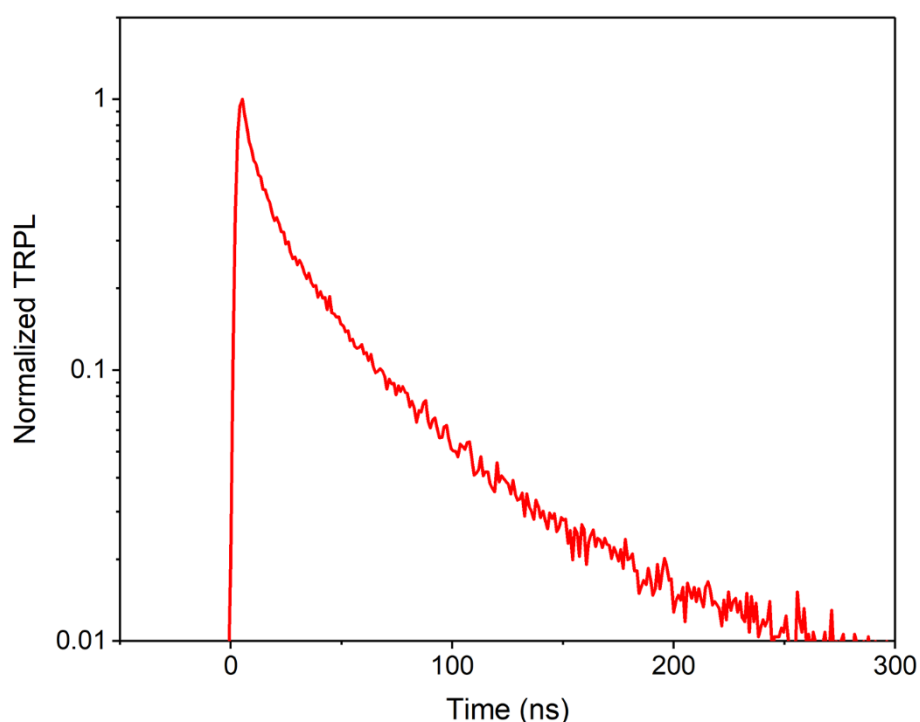


**Figure 13.** A typical time-resolved photoluminescence (TRPL) spectrum for an HCVD deposited perovskite with a carrier lifetime around 40 ns.<sup>[16]</sup> Published by The Royal Society of Chemistry.

Controversially to the higher stability with fewer defects in CVD deposited films, the shorter lifetime of carriers might be a result of the defects inside the bulk, instead of the defects at the grain boundaries. Such bulk defects may be the consequence of vapor deposition of precursors and/or the slow reaction rate between the gas and solid phase.<sup>[60]</sup> However, for the one-step solution coating process, the precursor is a colloid of small crystals in the solvent.<sup>[86]</sup> The crystal growth process is based on the nucleus, forming a high-quality grain inside the bulk with some defects around the boundaries. For the two-step solution coating process, the solvent and the ionized cations and anions might help the diffusion and reaction process, as shown in **Figure 12**. We hypothesize that there might be a small amount of  $\text{PbI}_2$  that does not fully convert into perovskite during CVD process. The unreacted  $\text{PbI}_2$  can stay inside the bulk, instead of at the grain boundaries, therefore may not be detected easily by XPS. Further research is needed to verify this point.

The other obvious difference between CVD-deposited and solution-coated films is the light absorbance. It has been observed that with the same film thickness, the CVD-deposited film is more transparent than the solution-coated film. The surface of the solution-coated film is also more mirror-like. Although there is no systematic research addressing this issue yet, we hypothesize that the reasons might be related to the surface morphology and grain size, and compactness. A more compact and smoother layer can be deposited using solution-based methods, which leads to mirror-like film surfaces.<sup>[70]</sup>

## **6. Modified CVD on textured surfaces for tandem solar cells**

Efficiency is one of the most important factors for a solar cell or solar module. By constructing tandem structure solar cells, PCE can be further improved over 30%.<sup>[87]</sup> The application of a perovskite/Si tandem cell is the most promising strategy.<sup>[88-89]</sup> In

these high-performance solar cells, optical management plays a vital role and the surface structure is important. A textured structure improves light harvesting. However, it is usually challenging to use traditional solution methods to coat a perovskite film on the textured surface.<sup>[89-90]</sup> Via coating a thick film on the textured Si substrate by a solution process, the textured structure is smoothened and maintains part of the anti-reflection properties.<sup>[90]</sup> It is reported that with a fully textured structure tandem solar cell, in which the perovskite was conformally deposited by a vacuum deposited  $\text{PbI}_2/\text{CsBr}$  and solution coated FAI/MAI, the current density loss due to reflection is reduced to  $1.64 \text{ mA/cm}^2$ , compared with a flat surface ( $3.14 \text{ mA/cm}^2$ ).<sup>[91]</sup> CVD is promising for the fabrication of the perovskite layer on textured substrates, as shown in **Figure 14**.<sup>[92]</sup> By measuring the thickness uniformity and reflectance of the perovskite film in a textured structure, the authors confirmed that a uniform and conformal coated film was obtained. In this work, Pb was introduced by sputtered  $\text{PbO}$ , following the conversion to perovskite in MAI vapor. Although a tandem solar cell with a CVD deposited conformal perovskite layer has not been reported yet, it holds great potential for the fully textured perovskite/silicon tandem solar cells/modules.<sup>[92]</sup>

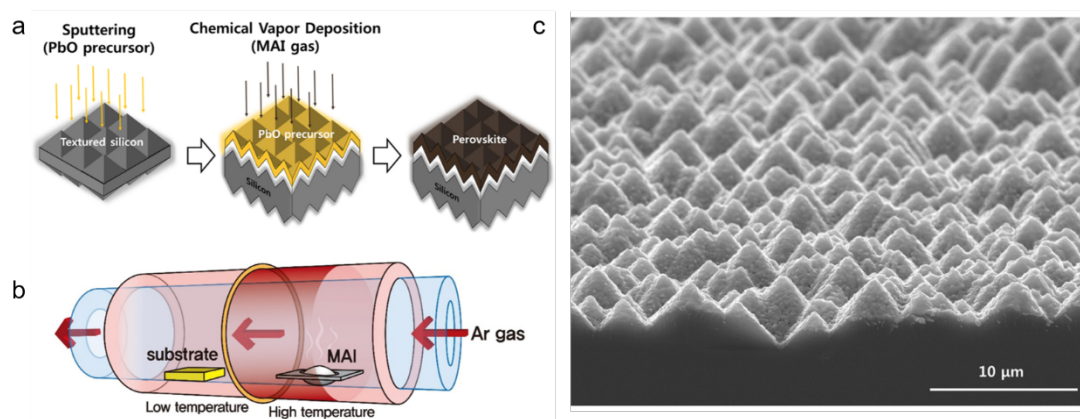


**Figure 14.** a, b) Schematic drawing and c) optical photo showing deposition of the perovskite film by hybrid CVD on a textured Si substrate. Reprinted from Ref. <sup>[92]</sup> with permission from Elsevier.

Considering the current density match in a perovskite/Si tandem solar cell, the

perovskite layer with a large bandgap of around 1.7-1.8 eV is required.<sup>[87, 89]</sup> Due to the versatile tuning of compositions, CVD is also suitable for large bandgap perovskite deposition. CsPbI<sub>3</sub> has been deposited on three different pyramidal size texture surfaces via CVD. It is shown that all the textured surfaces significantly reduce the reflectance by about 10%. Assuming a 100% internal quantum efficiency, this reduction of reflectance equals around 2 mA/cm<sup>2</sup> short-circuit density.<sup>[93]</sup> Further efforts are needed for CVD-deposited conformal pyramidal textured perovskite/Si tandem cells.

## 7. Modified CVD for flexible solar cells

CVD of perovskite is operated at a relatively low temperature below 160 °C, which is compatible with flexible substrates. Flexible perovskite thin films (CsPbBr<sub>3</sub>, and CsSnBr<sub>3</sub>) by CVD have been obtained.<sup>[20, 23]</sup> Although in these studies the perovskite films are used in photodetectors and resistive switching devices, they can also be used for the fabrication of flexible perovskite solar cells.

On the other hand, due to a conformal coating feature, CVD is useful for deposition of a perovskite layer on non-flat surfaces, such as on the surface of a fiber. An interesting fiber-shaped perovskite solar cell has been fabricated by the versatile CVD technique, with a PCE up to 10.79% (**Figure 15**).<sup>[80]</sup> Similar to the planar-type solar cells, the coating of porous PbI<sub>2</sub> around the fiber surface is needed for the effective diffusion of MAI vapor. The CVD helps the formation of high-quality perovskite layers on the curved fiber surface with a diameter of 250 μm, compared with the two-step solution-coating process. Currently the highest PCE is 10.79% for a fiber-shaped perovskite solar cell.<sup>[80]</sup>



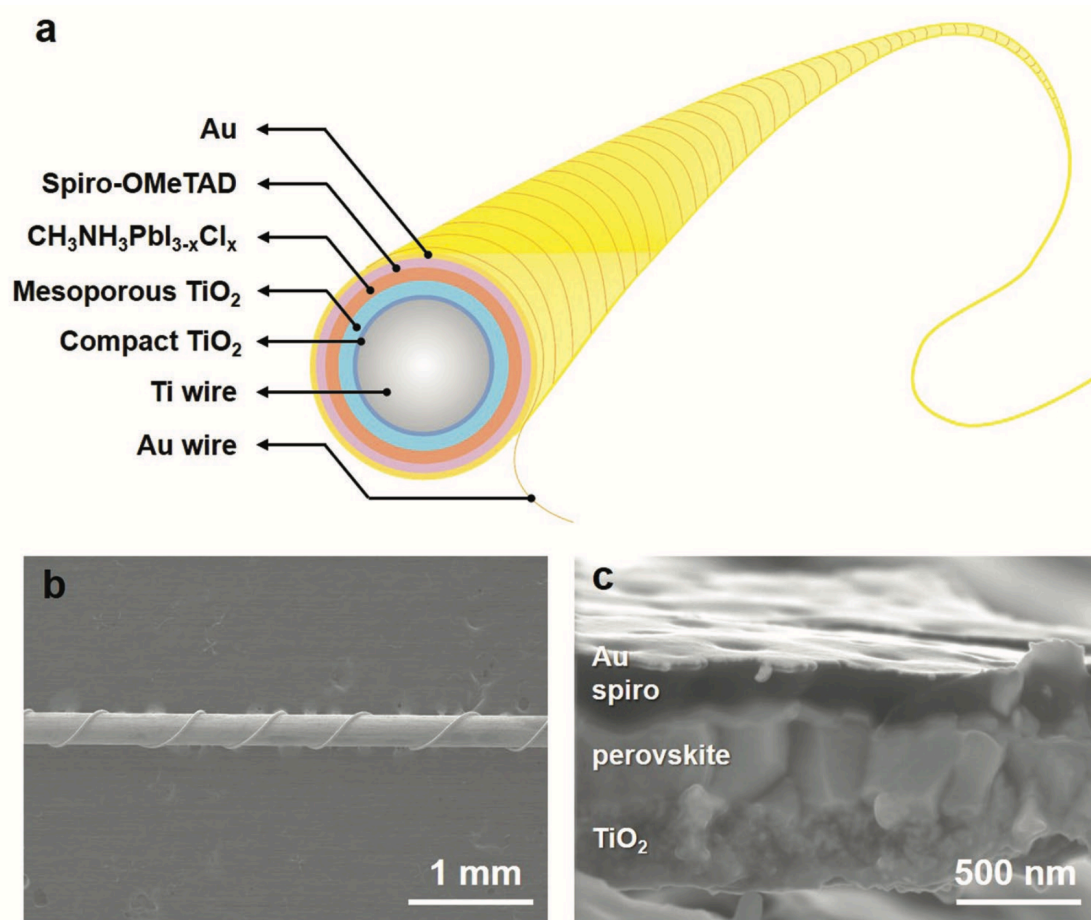


**Figure 15. a)** Schematic drawing and **b)** SEM image of fiber-shaped perovskite solar cells by CVD. **c)** Cross-section SEM image of CVD deposited perovskite solar cell on a curved fiber surface. Reproduced from Ref. <sup>[80]</sup> with permission from John Wiley and Sons.

## 8. Cost analysis regarding modified CVD and solution processing

When considering the cost-performance analysis, there are several stages: i) the fabrication cost for the perovskite solar module per m<sup>2</sup>, including the glass substrate, processing of perovskite solar module, frame, laminating film, junction-box and testing, which are so-called balanced of module (BOM); ii) taken into account the PCE of the resulting module, one needs to calculate the fabrication cost per peak watt energy power output; iii) assuming the lifetime of the module, combined with PCE degradation and average annual solar illumination, one needs to obtain the total energy output in the

1 entire working life and the calculation of levelized cost of electricity (LCOE). To  
2 compare the LCOE, the manufacturing cost of a solar module, the PCE of the resulting  
3 module and the operational lifetime all contribute to the final results. To compare  
4 perovskite solar module manufacturing cost by solution process and CVD process, we  
5 assume the same module structure with ITO as the substrate. The other components  
6 such as glass substrate, lamination film and junction-box are also the same. The  
7 materials cost is also assumed to be the same with the same module area.

8

9 There are several works on the cost-performance analysis of perovskite solar modules  
10 and tandem cells.<sup>[94-99]</sup> For the analysis, several assumptions need to be clarified, e.g.,  
11 the throughput/capacity of the factory (MW per year), factory operation time (hour per  
12 year), equipment footprint, factory location (in which country, the labor cost, footprint  
13 cost, installation cost, sales tax ext.), solar module efficiency (total area), solar module  
14 operational lifetime (degradation rate per year), and depreciation of equipment. Here in  
15 this review, we only focus on the manufacturing steps for perovskite layers. However,  
16 for the understanding of the difference, the idea for the cost-performance analysis and  
17 the above-mentioned assumptions should be noted. The cost for the equipment,  
18 maintenance, and the waste of raw materials will be taken into account.

19

20 Typically, the manufacturing cost for each square perovskite solar module is in the  
21 range of 37 to 140 dollars/m<sup>2</sup>.<sup>[94-96]</sup> Based on these reports, the processing cost of  
22 perovskite module structure only contributes to 24% of the total module cost, which  
23 consists of glass substrates, processing of perovskite solar module, frame, laminating  
24 film, junction-box and testing (**Figure 16a**). Furthermore, the coating of the perovskite  
25 layer contributes to only part of the processing of a perovskite solar module, and the  
26 cost for the fabrication of a p-i-n perovskite junction only contributes to 1.1% of the  
27 total cost (**Figure 16b**).<sup>[95]</sup> As calculated, the minimum sustainable prices (MSP) as a  
28 function of the assumed module efficiency is shown in **Figure 16c**. One should note

that this price is calculated without government subsidies, and this value is still lower than other mature photovoltaic techniques with subsidies.

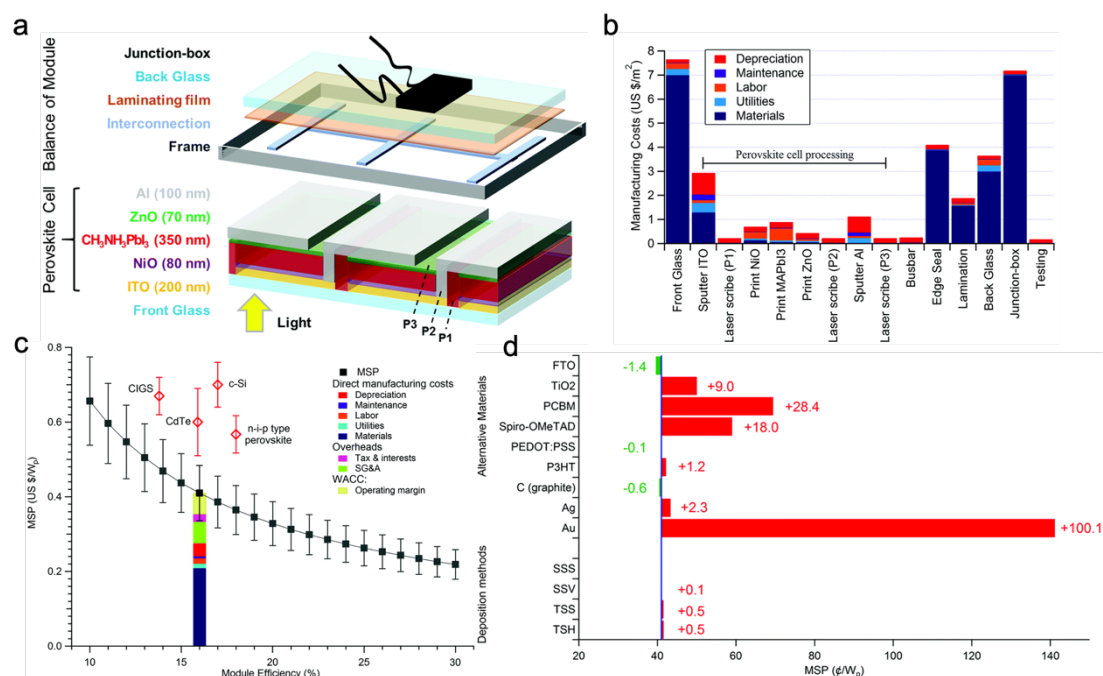


**Figure 16.** Cost-performance analysis of perovskite solar module in an inverted structure. **a)** Schematic drawing showing a completed perovskite solar module with perovskite cells and other required components. **b)** Manufacturing cost for each component of a completed perovskite solar module. **c)** MSP of perovskite solar modules as a function of efficiency and comparing with other mature photovoltaic technologies. **d)** The effect of changing perovskite materials and manufacturing process on the MSP. (SSS: single-step solution process; SSV: single-step vapor deposition process; TSS: two-step solution process; TSH: two-step hybrid process.) Reproduced from Ref [95] with permission from The Royal Society of Chemistry.

What we are interested in is how much the cost will be affected by changing the solution coating process to a CVD process. As shown in **Figure 16d**, the alternative of materials and processes for the manufacturing process has been provided. It can be seen that the changing of deposition process from one-step solution process to two-step hybrid deposition process, the MSP for selling only increased 0.5 cents/peak watt, which is

1 1.2% increase of the MSP.<sup>[95]</sup> Similarly, in another cost-analysis performance work by  
2 Han and coworkers, they assumed a 100 MW capacity of perovskite solar modules by  
3 a factory manufacturing thin-film silicon solar cells (60 MW), which are deposited by  
4 plasma-enhanced CVD. By changing the deposition process from a plasma-enhanced  
5 CVD process to a solution process, the initial capital investment decreased from 26  
6 million to 16 million dollars. However, when considering a rate of depreciation of 50%,  
7 the increase of cost based on the capital investment and manufacturing per peak watt is  
8 about 0.6 cents, on the 100 MW/year capacity.<sup>[99]</sup> This indicated that the application of  
9 CVD does not lead to much difference on the manufacturing cost of perovskite solar  
10 modules.

11  
12 Furthermore, the manufacturing cost for the two-terminal tandem solar module will  
13 only increase slightly due to the processing of a second subcell on the substrate. The  
14 manufacturing cost increased by  $\$5.1/\text{m}^2$ .<sup>[98]</sup> However, considering the output power  
15 increasing rate, the cost per peak watt is possible to be even lower. When considering  
16 the two-terminal tandem structure with a silicon subcell as substrate, and assuming an  
17 efficiency increase from 22.6% to 29.5% (the highest certified record for  
18 perovskite/silicon tandem cells), the output power under AM 1.5G increases from 226  
19  $\text{W}/\text{m}^2$  to 295  $\text{W}/\text{m}^2$ . The cost for high-efficiency crystalline heterojunction silicon solar  
20 cells is  $\$79.31/\text{m}^2$ .<sup>[100]</sup> The cost per peak watt further decreases by  $\$0.062/\text{peak watt}$ ,  
21 which indicates that the tandem structure is one of the promising structures for further  
22 reducing the cost of photovoltaic. As discussed in **Section 6**, CVD is of great potential  
23 for high-efficiency perovskite/silicon tandem solar cells with the textured structure,  
24 which is beneficial for light management and absorption.

## 25 26 **9. Conclusions and outlook**

27  
28 In this review article, we summarize the development of modified CVD for the

fabrication of perovskite solar cells and modules. This technique is promising for large-scale fabrication. A high efficiency approaching 20% has been achieved on a small area.<sup>[35]</sup> For future development, there are several potential directions. As summarized in **Table 1**, currently modified CVD based solar cells all use a regular n-i-p structure. An inverted structure has not been applied yet and might be a potential way to further improve the device performance and especially the operational stability. The second promising direction is application of the modified CVD methods for textured perovskite/silicon tandem solar cells, as introduced in **Section 6**. Further investigation on the rapid HCVD method to eliminate the extra ramping, cooling and stabilizing time may help improve the solar module efficiency as well as reducing cost. Modified CVD is promising for fabricating large-scale, low-cost perovskite solar cells with high stability. The cost for HCVD has a negligible effect on the levelized cost of energy compared with other solution coating processes, assuming the same module efficiency and lifetime. To further improve the stability and also efficiency, the defect passivation and interface modification are also important in modified CVD process. An attractive strategy is to combine the modified CVD and solution process together. For example, the defect passivation and interface modification for solution method can be applied in modified CVD deposited perovskite films. For example, solvent annealing post treatment,<sup>[101]</sup> the grain boundary self-passivation by MAI,<sup>[102]</sup> organic molecules,<sup>[103]</sup> cation exchange,<sup>[75]</sup> or other passivation additives such as FABr,<sup>[104]</sup> PEAI,<sup>[105]</sup> and recently bar-coated acetylcholine bromide,<sup>[106]</sup> and so on. Furthermore, considering the main differences between solution-coated and modified CVD deposited perovskite layers, in-depth investigations are needed to reveal the underlying mechanisms responsible for shorter carrier lifetime and lower efficiency for modified CVD deposited perovskite solar cells.

## Acknowledgments

L. Q. acknowledges the funding by National Natural Science Foundation of China

(NSFC) (22109067), and the research start-up grant by Southern University of Science and Technology. S. H. acknowledges the funding by NSFC (52103300), and start-up fund from Harbin Institute of Technology (Shenzhen) (HA45001121). Y. J. acknowledges the funding support from the Energy Materials and Optoelectronics Unit of Songshan Lake Materials Laboratory. Y. B. Q. acknowledges the support from the Energy Materials and Surface Sciences Unit of the Okinawa Institute of Science and Technology Graduate University.

## Reference

- [1] M. A. Green, E. D. Dunlop, J. Hohl - Ebinger, M. Yoshita, N. Kopidakis, X. Hao, *Prog. Photovolt. Res. Appl.* **2021**, 29, 657-667.
- [2] T. Wu, Z. Qin, Y. Wang, Y. Wu, W. Chen, S. Zhang, M. Cai, S. Dai, J. Zhang, J. Liu, Z. Zhou, X. Liu, H. Segawa, H. Tan, Q. Tang, J. Fang, Y. Li, L. Ding, Z. Ning, Y. B. Qi, Y. Zhang, L. Han, *Nanomicro Lett.* **2021**, 13, 152.
- [3] L. Qiu, S. He, L. K. Ono, S. Liu, Y. B. Qi, *ACS Energy Lett.* **2019**, 4, 2147-2167.
- [4] W. Tress, *Adv. Energy Mater.* **2017**, 7, 1602358.
- [5] N.-G. Park, K. Zhu, *Nat. Rev. Mater.* **2020**, 5, 333-350.
- [6] Z. Li, T. R. Klein, D. H. Kim, M. Yang, J. J. Berry, M. F. A. M. van Hest, K. Zhu, *Nat. Rev. Mater.* **2018**, 3, 18017.
- [7] Y. Vaynzof, *Adv. Energy Mater.* **2020**, 10, 2003073.
- [8] M. R. Leyden, L. K. Ono, S. R. Raga, Y. Kato, S. Wang, Y. B. Qi, *J. Mater. Chem. A* **2014**, 2, 18742-18745.
- [9] P. Luo, Z. Liu, W. Xia, C. Yuan, J. Cheng, Y. Lu, *ACS Appl. Mater. Interfaces* **2015**, 7, 2708-2714.
- [10] M. R. Leyden, Y. Jiang, Y. B. Qi, *J. Mater. Chem. A* **2016**, 4, 13125-13132.
- [11] X. Liu, L. Cao, Z. Guo, Y. Li, W. Gao, L. Zhou, *Materials* **2019**, 12, 3304.
- [12] P. Luo, S. Zhou, W. Xia, J. Cheng, C. Xu, Y. Lu, *Adv. Mater. Interfaces* **2017**, 4, 1600970.
- [13] D. J. Lewis, P. O'Brien, *Chem. Commun.* **2014**, 50, 6319-6321.
- [14] S. T. Ha, X. Liu, Q. Zhang, D. Giovanni, T. C. Sum, Q. Xiong, *Adv. Optical Mater.* **2014**, 2, 838-844.
- [15] G. Kim, S. An, S.-K. Hyeong, S.-K. Lee, M. Kim, N. Shin, *Chem. Mater.* **2019**, 31, 8212-8221.
- [16] L. Qiu, S. He, Y. Jiang, D.-Y. Son, L. K. Ono, Z. Liu, T. Kim, T. Bouloumis, S. Kazaoui, Y. B. Qi, *J. Mater. Chem. A* **2019**, 7, 6920-6929.
- [17] L. Qiu, S. He, Z. Liu, L. K. Ono, D.-Y. Son, Y. Liu, G. Tong, Y. B. Qi, *J. Mater. Chem. A* **2020**, 8, 23404-23412.
- [18] M. R. Leyden, L. Meng, Y. Jiang, L. K. Ono, L. Qiu, E. J. Juarez-Perez, C. Qin,

- 1 C. Adachi, Y. B. Qi, *J. Phys. Chem. Lett.* **2017**, *8*, 3193-3198.
- 2 [19] G. Tong, X. Geng, Y. Yu, L. Yu, J. Xu, Y. Jiang, Y. Sheng, Y. Shi, K. Chen, *RSC*  
3 *Adv.* **2017**, *7*, 18224-18230.
- 4 [20] X. Li, X. Mo, Y. Xiang, G. Dai, P. He, M. Fang, J. Sun, H. Huang, J. Yang, *J.*  
5 *Phys. D: Appl. Phys.* **2020**, *53*, 354002.
- 6 [21] S. V. N. Pammi, R. Maddaka, V.-D. Tran, J.-H. Eom, V. Pecunia, S. Majumder,  
7 M.-D. Kim, S. G. Yoon, *Nano Energy* **2020**, *74*, 104872.
- 8 [22] H.-D. Kim, S. V. N. Pammi, H.-W. Lee, S. W. Lee, S.-G. Yoon, J. Park, Y. J.  
9 Kim, H.-S. Kim, *J. Alloys Compd.* **2020**, *815*, 152404.
- 10 [23] H. Wang, J. Lin, Y. Zhu, X. Zeng, H. Wei, P. Cheng, H. Lu, Y. Liu, R. Xiong,  
11 *Adv. Electron. Mater.* **2020**, *6*, 2000799.
- 12 [24] P. Luo, Z. Liu, W. Xia, C. Yuan, J. Cheng, Y. Lu, *J. Mater. Chem. A* **2015**, *3*,  
13 12443-12451.
- 14 [25] M. M. Tavakoli, L. Gu, Y. Gao, C. Reckmeier, J. He, A. L. Rogach, Y. Yao, Z.  
15 Fan, *Sci. Rep.* **2015**, *5*, 14083.
- 16 [26] C.-R. Ke, D. J. Lewis, A. S. Walton, Q. Chen, B. F. Spencer, M. Z. Mokhtar, C.  
17 L. Compean-Gonzalez, P. O'Brien, A. G. Thomas, W. R. Flavell, *ACS Appl.*  
18 *Energy Mater.* **2019**, *2*, 6012-6022.
- 19 [27] J. Yin, H. Qu, J. Cao, H. Tai, J. Li, N. Zheng, *J. Mater. Chem. A* **2016**, *4*, 13203-  
20 13210.
- 21 [28] C. Mortan, T. Hellmann, M. Buchhorn, M. d'Eril Melzi, O. Clemens, T. Mayer,  
22 W. Jaegermann, *Energy Sci. Eng.* **2020**, *8*, 3165-3173.
- 23 [29] Y. Jiang, M. Remeika, Z. Hu, E. J. Juarez - Perez, L. Qiu, Z. Liu, T. Kim, L. K.  
24 Ono, D. Y. Son, Z. Hawash, M. R. Leyden, Z. Wu, L. Meng, J. Hu, Y. B. Qi,  
25 *Adv. Energy Mater.* **2019**, *9*, 1803047.
- 26 [30] A. Ioakeimidis, C. Christodoulou, M. Lux-Steiner, K. Fostiropoulos, *J. Solid*  
27 *State Chem.* **2016**, *244*, 20-24.
- 28 [31] A. Ng, Z. Ren, Q. Shen, S. H. Cheung, H. C. Gokkaya, S. K. So, A. B. Djuricic,  
29 Y. Wan, X. Wu, C. Surya, *ACS Appl. Mater. Interfaces* **2016**, *8*, 32805-32814.
- 30 [32] G. Kim, H. Min, K. S. Lee, D. Y. Lee, S. M. Yoon, S. I. Seok, *Science* **2020**,  
31 *370*, 108-112.
- 32 [33] J. J. Yoo, G. Seo, M. R. Chua, T. G. Park, Y. Lu, F. Rotermund, Y.-K. Kim, C.  
33 S. Moon, N. J. Jeon, J.-P. Correa-Baena, V. Bulović, S. S. Shin, M. G. Bawendi,  
34 J. Seo, *Nature* **2021**, *590*, 587-593.
- 35 [34] M. R. Leyden, M. V. Lee, S. R. Raga, Y. B. Qi, *J. Mater. Chem. A* **2015**, *3*,  
36 16097-16103.
- 37 [35] H. Lu, Y. Liu, P. Ahlawat, A. Mishra, W. R. Tress, F. T. Eickemeyer, Y. Yang, F.  
38 Fu, Z. Wang, C. E. Avalos, B. I. Carlsen, A. Agarwalla, X. Zhang, X. Li, Y. Zhan,  
39 S. M. Zakeeruddin, L. Emsley, U. Rothlisberger, L. Zheng, A. Hagfeldt, M.  
40 Grätzel, *Science* **2020**, *370*, eabb8985.
- 41 [36] L. Luo, Z. Ku, W. Li, X. Zheng, X. Li, F. Huang, Y. Peng, L. Ding, Y.-B. Cheng,  
42 *Sci. Bull.* **2021**, *66*, 962-964.

- 1 [37] D. S. Bhachu, D. O. Scanlon, E. J. Saban, H. Bronstein, I. P. Parkin, C. J.  
2 Carmalt, R. G. Palgrave, *J. Mater. Chem. A* **2015**, 3, 9071-9073.
- 3 [38] Y. Peng, G. Jing, T. Cui, *J. Mater. Chem. A* **2015**, 3, 12436-12442.
- 4 [39] Q. Chen, H. Zhou, Z. Hong, S. Luo, H.-S. Duan, H.-H. Wang, Y. Liu, G. Li, Y.  
5 Yang, *J. Am. Chem. Soc.* **2014**, 136, 622-625.
- 6 [40] L. Luo, Y. Zhang, N. Chai, X. Deng, J. Zhong, F. Huang, Y. Peng, Z. Ku, Y.-B.  
7 Cheng, *J. Mater. Chem. A* **2018**, 6, 21143-21148.
- 8 [41] X. Zhu, D. Yang, R. Yang, B. Yang, Z. Yang, X. Ren, J. Zhang, J. Niu, J. Feng,  
9 S. F. Liu, *Nanoscale* **2017**, 9, 12316-12323.
- 10 [42] G. Tong, H. Li, G. Li, T. Zhang, C. Li, L. Yu, J. Xu, Y. Jiang, Y. Shi, K. Chen,  
11 *Nano Energy* **2018**, 48, 536-542.
- 12 [43] P. Luo, S. Zhou, Y. Zhou, W. Xia, L. Sun, J. Cheng, C. Xu, Y. Lu, *ACS Appl.*  
13 *Mater. Interfaces* **2017**, 9, 42708-42716.
- 14 [44] X. Deng, J. Hua, F. Huang, Y. Peng, W. Li, Z. Ku, Y.-b. Cheng, *Sustain. Energy*  
15 *Fuels* **2020**, 4, 2491-2496.
- 16 [45] X. Chen, Y. Myung, A. Thind, Z. Gao, B. Yin, M. Shen, S. B. Cho, P. Cheng, B.  
17 Sadtler, R. Mishra, P. Banerjee, *J. Mater. Chem. A* **2017**, 5, 24728-24739.
- 18 [46] X. Mo, X. Li, G. Dai, P. He, J. Sun, H. Huang, J. Yang, *Nanoscale* **2019**, 11,  
19 21386-21393.
- 20 [47] S. Chen, J. Briscoe, Y. Shi, K. Chen, R. M. Wilson, S. Dunn, R. Binions,  
21 *CrystEngComm* **2015**, 17, 7486-7489.
- 22 [48] M. Afzaal, H. M. Yates, *Surf. Coat. Technol.* **2017**, 321, 336-340.
- 23 [49] M. Afzaal, B. Salhi, A. Al-Ahmed, H. M. Yates, A. S. Hakeem, *J. Mater. Chem.*  
24 *C* **2017**, 5, 8366-8370.
- 25 [50] H. Nishinaka, M. Yoshimoto, *Jpn. J. Appl. Phys.* **2016**, 55, 100308.
- 26 [51] M. Aamir, M. Sher, M. D. Khan, M. A. Malik, J. Akhtar, N. Revaprasadu, *Mater.*  
27 *Lett.* **2017**, 190, 244-247.
- 28 [52] S. Basak, M. Afzaal, H. M. Yates, *Mater. Chem. Phys.* **2019**, 223, 157-163.
- 29 [53] J. C.-R. Ke, D. J. Lewis, A. S. Walton, B. F. Spencer, P. O'Brien, A. G. Thomas,  
30 W. R. Flavell, *J. Mater. Chem. A* **2018**, 6, 11205-11214.
- 31 [54] Y. Wu, A. Islam, X. Yang, C. Qin, J. Liu, K. Zhang, W. Peng, L. Han, *Energy*  
32 *Environ. Sci.* **2014**, 7, 2934-2938.
- 33 [55] S. R. Raga, L. K. Ono, Y. B. Qi, *J. Mater. Chem. A* **2016**, 4, 2494-2500.
- 34 [56] Z. Liu, L. Qiu, E. J. Juarez-Perez, Z. Hawash, T. Kim, Y. Jiang, Z. Wu, S. R.  
35 Raga, L. K. Ono, S. F. Liu, Y. B. Qi, *Nat. Commun.* **2018**, 9, 3880.
- 36 [57] F. Wang, H. Yu, H. Xu, N. Zhao, *Adv. Funct. Mater.* **2015**, 25, 1120-1126.
- 37 [58] Y. Wang, X. Guan, D. Li, H.-C. Cheng, X. Duan, Z. Lin, X. Duan, *Nano Res.*  
38 **2017**, 10, 1223-1233.
- 39 [59] T. Che, C. Shen, J. Gao, X. Ji, W. Kong, Y. Liu, *Opt. Mater.* **2020**, 107, 110120.
- 40 [60] T. Moser, K. Artuk, Y. Jiang, T. Feurer, E. Gilshtein, A. N. Tiwari, F. Fu, *J. Mater.*  
41 *Chem. A* **2020**, 8, 21973-21982.
- 42 [61] L. Qiu, Z. Liu, L. K. Ono, Y. Jiang, D. Y. Son, Z. Hawash, S. He, Y. B. Qi, *Adv.*



- 1 *Funct. Mater.* **2019**, *29*, 1806779.
- 2 [62] M. Batzill, K. Katsiev, J. M. Burst, U. Diebold, A. M. Chaka, B. Delley, *Phys.*  
3 *Rev. B* **2005**, *72*, 165414.
- 4 [63] M. Batzill, *Sensors* **2006**, *6*, 1345-1366.
- 5 [64] T. Bu, J. Li, H. Li, C. Tian, J. Su, G. Tong, L. K. Ono, C. Wang, Z. Lin, N. Chai,  
6 X. L. Zhang, J. Chang, J. Lu, J. Zhong, W. Huang, Y. B. Qi, Y. B. Cheng, F.  
7 Huang, *Science* **2021**, *372*, 1327-1332.
- 8 [65] C. Niu, C. Wang, G. Zhang, Q. Zhao, C. Fang, W. Li, F. Huang, Z. Ku, Y.-b.  
9 Cheng, *Solar RRL* **2021**, *5*, 2100102.
- 10 [66] X. Wei, Y. Peng, G. Jing, T. Cui, *Jpn. J. Appl. Phys.* **2018**, *57*, 052301.
- 11 [67] M. H. Li, H. H. Yeh, Y. H. Chiang, U. S. Jeng, C. J. Su, H. W. Shiu, Y. J. Hsu,  
12 N. Kosugi, T. Ohigashi, Y. A. Chen, P. S. Shen, P. Chen, T. F. Guo, *Adv. Mater.*  
13 **2018**, *30*, e1801401.
- 14 [68] X. Li, D. Lin, Z. Chen, Z. Li, J. Wang, J. Chen, L. Gong, J. Xu, K. Chen, P. Liu,  
15 W. Xie, *ACS Appl. Energy Mater.* **2020**, *3*, 6544-6551.
- 16 [69] C. P. Clark, B. Voigt, E. S. Aydil, R. J. Holmes, *Sustain. Energy Fuels* **2019**, *3*,  
17 2447-2455.
- 18 [70] A. F. Akbulatov, L. A. Frolova, S. A. Tsarev, I. Zhidkov, S. Y. Luchkin, E. Z.  
19 Kurmaev, K. J. Stevenson, S. M. Aldoshin, P. A. Troshin, *J. Phys. Chem. C* **2020**,  
20 *124*, 21378-21385.
- 21 [71] Y. Li, J. K. Cooper, R. Buonsanti, C. Giannini, Y. Liu, F. M. Toma, I. D. Sharp,  
22 *J. Phys. Chem. Lett.* **2015**, *6*, 493-499.
- 23 [72] P.-S. Shen, J.-S. Chen, Y.-H. Chiang, M.-H. Li, T.-F. Guo, P. Chen, *Adv. Mater.*  
24 *Interfaces* **2016**, *3*, 1500849.
- 25 [73] H. C. Gokkaya, S. Qian, Z. W. Ren, A. Ng, C. Surya, *Ieee. Phot. Spec. Conf.*  
26 **2017**, 958-962.
- 27 [74] W. G. Choi, D. W. Kang, S. Na, C. G. Park, F. P. Gokdemir, T. Moon, *Nanoscale*  
28 *Res. Lett.* **2018**, *13*, 9.
- 29 [75] Y. Jiang, M. R. Leyden, L. Qiu, S. Wang, L. K. Ono, Z. Wu, E. J. Juarez-Perez,  
30 Y. B. Qi, *Adv. Funct. Mater.* **2018**, *28*, 1703835.
- 31 [76] P. Luo, Y. Zhou, S. Zhou, Y. Lu, C. Xu, W. Xia, L. Sun, *Chem. Eng. J.* **2018**,  
32 *343*, 146-154.
- 33 [77] Q. Shen, A. Ng, Z. Ren, H. C. Gokkaya, A. B. Djuricic, J. A. Zapien, C. Surya,  
34 *ACS Appl. Mater. Interfaces* **2018**, *10*, 371-380.
- 35 [78] V.-D. Tran, S. V. N. Pammi, V.-D. Dao, H.-S. Choi, S.-G. Yoon, *J. Alloys Compd.*  
36 **2018**, *747*, 703-711.
- 37 [79] J. Chen, J. Xu, C. Zhao, B. Zhang, X. Liu, S. Dai, J. Yao, *ACS Appl. Mater.*  
38 *Interfaces* **2019**, *11*, 4597-4606.
- 39 [80] B. Dong, J. Hu, X. Xiao, S. Tang, X. Gao, Z. Peng, D. Zou, *Adv. Mater. Technol.*  
40 **2019**, *4*, 1900131.
- 41 [81] S. Sanders, D. Stummler, P. Pfeiffer, N. Ackermann, G. Simkus, M. Heuken, P.  
42 K. Baumann, A. Vescan, H. Kalisch, *Sci. Rep.* **2019**, *9*, 9774.

- 1 [82] C. Yang, X. Shan, T. Xie, *Energies* **2019**, *12*, 4508.
- 2 [83] S. Draguta, S. Thakur, Y. V. Morozov, Y. Wang, J. S. Manser, P. V. Kamat, M.  
3 Kuno, *J. Phys. Chem. Lett.* **2016**, *7*, 715-721.
- 4 [84] S. V. N. Pammi, H.-W. Lee, J.-H. Eom, S.-G. Yoon, *ACS Appl. Energy Mater.*  
5 **2018**, *1*, 3301-3312.
- 6 [85] M. Stolterfoht, C. M. Wolff, J. A. Márquez, S. Zhang, C. J. Hages, D. Rothhardt,  
7 S. Albrecht, P. L. Burn, P. Meredith, T. Unold, D. Neher, *Nat. Energy* **2018**, *3*,  
8 847-854.
- 9 [86] Z. Yang, W. Zhang, S. Wu, H. Zhu, Z. Liu, Z. Liu, Z. Jiang, R. Chen, J. Zhou,  
10 Q. Lu, Z. Xiao, L. Shi, H. Chen, L. K. Ono, S. Zhang, Y. Zhang, Y. B. Qi, L.  
11 Han, W. Chen, *Sci. Adv.* **2021**, *7*, eabg3749.
- 12 [87] T. Leijtens, K. A. Bush, R. Prasanna, M. D. McGehee, *Nat. Energy* **2018**, *3*,  
13 828-838.
- 14 [88] A. Al-Ashouri, E. Kohnen, B. Li, A. Magomedov, H. Hempel, P. Caprioglio, J.  
15 A. Marquez, A. B. Morales Vilches, E. Kasparavicius, J. A. Smith, N. Phung, D.  
16 Menzel, M. Grischek, L. Kegelmann, D. Skroblin, C. Gollwitzer, T.  
17 Malinauskas, M. Jost, G. Matic, B. Rech, R. Schlatmann, M. Topic, L. Korte,  
18 A. Abate, B. Stannowski, D. Neher, M. Stolterfoht, T. Unold, V. Getautis, S.  
19 Albrecht, *Science* **2020**, *370*, 1300-1309.
- 20 [89] Y. Hou, E. Aydin, M. De Bastiani, C. Xiao, F. H. Isikgor, D. J. Xue, B. Chen, H.  
21 Chen, B. Bahrami, A. H. Chowdhury, A. Johnston, S. W. Baek, Z. Huang, M.  
22 Wei, Y. Dong, J. Troughton, R. Jalmood, A. J. Mirabelli, T. G. Allen, E. Van  
23 Kerschaver, M. I. Saidaminov, D. Baran, Q. Qiao, K. Zhu, S. De Wolf, E. H.  
24 Sargent, *Science* **2020**, *367*, 1135-1140.
- 25 [90] B. Chen, Z. J. Yu, S. Manzoor, S. Wang, W. Weigand, Z. Yu, G. Yang, Z. Ni, X.  
26 Dai, Z. C. Holman, J. Huang, *Joule* **2020**, *4*, 850-864.
- 27 [91] F. Sahli, J. Werner, B. A. Kamino, M. Brauning, R. Monnard, B. Paviet-  
28 Salomon, L. Barraud, L. Ding, J. J. Diaz Leon, D. Sacchetto, G. Cattaneo, M.  
29 Despeisse, M. Boccard, S. Nicolay, Q. Jeangros, B. Niesen, C. Ballif, *Nat. Mater.*  
30 **2018**, *17*, 820-826.
- 31 [92] J.-K. Hwang, S.-W. Lee, W. Lee, S. Bae, K. Cho, S. Kim, S. Lee, J. Y. Hyun, Y.  
32 Kang, H.-S. Lee, D. Kim, *Thin Solid Films* **2020**, *693*, 137694.
- 33 [93] K. Hamada, K. Yonezawa, K. Yamamoto, T. Taima, S. Hayase, N. Ooyagi, Y.  
34 Yamamoto, K. Ohdaira, *Jpn. J. Appl. Phys.* **2019**, *58*, Sbbf06.
- 35 [94] N. L. Chang, A. W. Yi Ho-Baillie, P. A. Basore, T. L. Young, R. Evans, R. J.  
36 Egan, *Prog. Photovolt. Res. Appl.* **2017**, *25*, 390-405.
- 37 [95] Z. Song, C. L. McElvany, A. B. Phillips, I. Celik, P. W. Krantz, S. C. Watthage,  
38 G. K. Liyanage, D. Apul, M. J. Heben, *Energy Environ. Sci.* **2017**, *10*, 1297-  
39 1305.
- 40 [96] N. L. Chang, A. W. Y. Ho-Baillie, D. Vak, M. Gao, M. A. Green, R. J. Egan, *Sol.*  
41 *Energy Mater. Sol. Cells* **2018**, *174*, 314-324.
- 42 [97] Z. Li, Y. Zhao, X. Wang, Y. Sun, Z. Zhao, Y. Li, H. Zhou, Q. Chen, *Joule* **2018**,

2, 1559-1572.

[98] Z. Song, A. B. Phillips, I. Celik, G. K. Liyanage, D. Zhao, D. Apul, Y. Yan, M. J. Heben, in *2018 IEEE 7th World Conference on Photovoltaic Energy Conversion (WCPEC) (A Joint Conference of 45th IEEE PVSC, 28th PVSEC & 34th EU PVSEC)*, **2018**, pp. 1134-1138.

[99] M. Cai, Y. Wu, H. Chen, X. Yang, Y. Qiang, L. Han, *Adv. Sci.* **2017**, *4*, 1600269.

[100] S. E. Sofia, H. Wang, A. Bruno, J. L. Cruz-Campa, T. Buonassisi, I. M. Peters, *Sustain. Energy Fuels* **2020**, *4*, 852-862.

[101] Z. Xiao, Q. Dong, C. Bi, Y. Shao, Y. Yuan, J. Huang, *Adv. Mater.* **2014**, *26*, 6503-6509.

[102] Z. Hawash, S. R. Raga, D.-Y. Son, L. K. Ono, N.-G. Park, Y. B. Qi, *J. Phys. Chem. Lett.* **2017**, *8*, 3947-3953.

[103] D.-H. Kang, S.-Y. Kim, J.-W. Lee, N.-G. Park, *J. Mater. Chem. A* **2021**, *9*, 3441-3450.

[104] S. Xiao, Y. Li, S. Zheng, S. Yang, *MRS Bulletin* **2020**, *45*, 431-438.

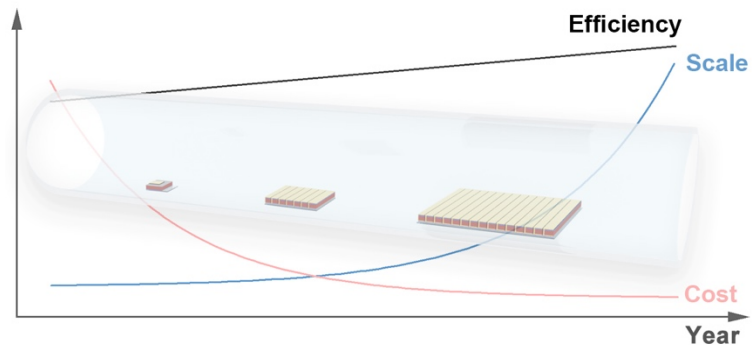
[105] Q. Jiang, Y. Zhao, X. W. Zhang, X. L. Yang, Y. Chen, Z. M. Chu, Q. F. Ye, X. X. Li, Z. G. Yin, J. B. You, *Nat. Photonics* **2019**, *13*, 460-466.

[106] J. W. Yoo, J. Jang, U. Kim, Y. Lee, S.-G. Ji, E. Noh, S. Hong, M. Choi, S. I. Seok, *Joule* **2021**, *5*, 2420-2436.

1

## Table of contents entry

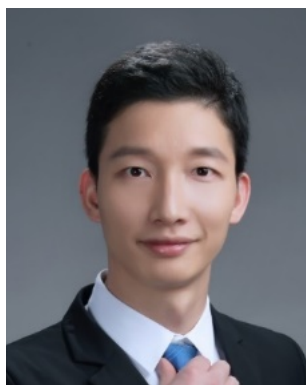
2



3

4

5 Modified chemical vapor deposition as a high throughput, low-cost method for  
6 fabricating scalable and stable perovskite solar cells/modules has been reviewed  
7 comprehensively, with potential future development perspectives.



1  
2  
3  
4  
5  
6  
7  
8  
9

**Longbin Qiu** is an Assistant Professor in Southern University of Science and Technology in China. He received his B.E. (2011) and Ph.D. (2016) from Sun Yat-sen University and Fudan University, respectively. He conducted his postdoctoral research in Energy Materials and Surface Sciences Unit at Okinawa Institute of Science and Technology Graduate University in Japan during 2016-2020. His current interests focus on the flexible and wearable electronics, and scalable and stable photovoltaic devices.

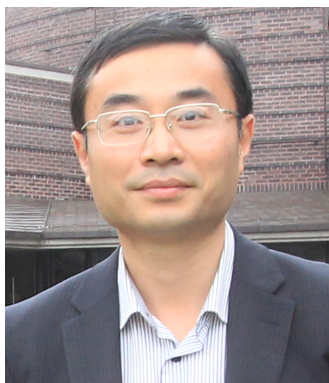


10  
11  
12  
13  
14  
15  
16  
17  
18

**Sisi He** is an Associate Professor at Harbin Institute of Technology (Shenzhen) in China. She received her B.E. (2011), M.S. (2014) and Ph.D. (2017) from Northeastern University, Tianjin University and Fudan University, respectively, and then joined Okinawa Institute of Science and Technology Graduate University, Japan and MacMaster University, Canada as a postdoctoral research fellow during 2018-2021. Her current interests focus on flexible devices including sensor/energy storage and conversion platform.



**Yan Jiang** a Professor at Songshan Lake Materials Laboratory. He received his B.S. and Ph.D. from Sun Yat-Sen University and Institute of Chemistry Chinese Academy of Science, respectively. Between 2015 and 2020, he worked at Okinawa Institute of Science and Technology Graduate University and Swiss Federal Laboratories for Materials Science and Technology as a postdoctoral scholar. His research focuses on next-generation high-performance energy harvesting materials and devices.



**Yabing Qi** is Professor and Unit Director of Energy Materials and Surface Sciences Unit at Okinawa Institute of Science and Technology Graduate University in Japan, and a Fellow of the Royal Society of Chemistry. He received his B.S., M.Phil., and Ph.D. from Nanjing University, Hong Kong University of Science and Technology, and UC Berkeley, respectively. His research interests include surface / interface sciences, perovskite solar cells, lithium batteries, organic electronics, energy materials and devices (<https://groups.oist.jp/emssu>).